SANDIA REPORT
SAND2014-15588
Unlimited Release
Printed July 2014

Structural Health and Prognostics Management for Offshore Wind Turbines: Sensitivity Analysis of Rotor Fault and Blade Damage with O&M Cost Modeling

Noah J. Myrent, Natalie C. Barrett, Douglas E. Adams, and D. Todd Griffith

Prepared by
Sandia National Laboratories
Albuquerque, New Mexico 87185 and Livermore, California 94550

Sandia National Laboratories is a multi-program laboratory managed and operated by Sandia Corporation, a wholly owned subsidiary of Lockheed Martin Corporation, for the U.S. Department of Energy's National Nuclear Security Administration under contract DE-AC04-94AL85000.

Approved for public release; further dissemination unlimited.

Issued by Sandia National Laboratories, operated for the United States Department of Energy by Sandia Corporation.

NOTICE: This report was prepared as an account of work sponsored by an agency of the United States Government. Neither the United States Government, nor any agency thereof, nor any of their employees, nor any of their contractors, subcontractors, or their employees, make any warranty, express or implied, or assume any legal liability or responsibility for the accuracy, completeness, or usefulness of any information, apparatus, product, or process disclosed, or represent that its use would not infringe privately owned rights. Reference herein to any specific commercial product, process, or service by trade name, trademark, manufacturer, or otherwise, does not necessarily constitute or imply its endorsement, recommendation, or favoring by the United States Government, any agency thereof, or any of their contractors or subcontractors. The views and opinions expressed herein do not necessarily state or reflect those of the United States Government, any agency thereof, or any of their contractors.

Printed in the United States of America. This report has been reproduced directly from the best available copy.

Available to DOE and DOE contractors from

U.S. Department of Energy
Office of Scientific and Technical Information
P.O. Box 62
Oak Ridge, TN 37831

Telephone: (865) 576-8401
Facsimile: (865) 576-5728
E-Mail: reports@adonis.osti.gov
Online ordering: http://www.osti.gov/bridge

Available to the public from

U.S. Department of Commerce
National Technical Information Service
5285 Port Royal Rd.
Springfield, VA 22161

Telephone: (800) 553-6847
Facsimile: (703) 605-6900
E-Mail: orders@ntis.fedworld.gov
Online order: http://www.ntis.gov/help/ordermethods.asp?loc=7-4-0#online

SAND2014-15588
Unlimited Release
Printed July 2014

Structural Health and Prognostics Management for Offshore Wind Turbines: Sensitivity Analysis of Rotor Fault and Blade Damage with O&M Cost Modeling

Noah J. Myrent, Natalie C. Barrett, and Douglas E. Adams,
Vanderbilt Laboratory for Systems Integrity & Reliability
566 Mainstream Dr.
Nashville, TN 37228

D. Todd Griffith
Wind Energy Technology Department
Sandia National Laboratories
P.O. Box 5800
Albuquerque, New Mexico 87185-MS1124

Abstract

Operations and maintenance costs for offshore wind plants are significantly higher than the current costs for land-based (onshore) wind plants. One way to reduce these costs would be to implement a structural health and prognostic management (SHPM) system as part of a condition based maintenance paradigm with smart load management and utilize a state-based cost model to assess the economics associated with use of the SHPM system. To facilitate the development of such a system a multi-scale modeling and simulation approach developed in prior work is used to identify how the underlying physics of the system are affected by the presence of damage and faults, and how these changes manifest themselves in the operational response of a full turbine. This methodology was used to investigate two case studies: (1) the effects of rotor imbalance due to pitch error (aerodynamic imbalance) and mass imbalance and (2) disbond of the shear web; both on a 5-MW offshore wind turbine in the present report. Sensitivity analyses were carried out for the detection strategies of rotor imbalance and shear web disbond developed in prior work by evaluating the robustness of key measurement parameters in the presence of varying wind speeds, horizontal shear, and turbulence. Detection strategies were refined for these fault mechanisms and probabilities of detection were calculated. For all three fault mechanisms, the probability of detection was 96% or higher for the optimized wind speed ranges of the laminar, 30% horizontal shear, and 60% horizontal shear wind profiles. The revised cost model provided insight into the estimated savings in operations and maintenance costs as they relate to the characteristics of the SHPM system. The integration of the health monitoring information and O&M cost versus damage/fault severity information provides the initial steps to identify processes to reduce operations and maintenance costs for an offshore wind farm while increasing turbine availability, revenue, and overall profit.

CONTENTS

FIGURES

TABLES

NOMENCLATURE

AEP	annual energy production
BEM	Blade Element Momentum
BPE	Beam Property Extraction
CBM	condition based maintenance
COE	cost of energy
dB	decibel
DOE	Department of Energy
DOWEC	Dutch Offshore Wind Energy Converter Project
FAST	Fatigue, Aerodynamics, Structures, and Turbulence
FCR	fixed charge rate
FEA	Finite Element Analysis
HAWT	horizontal axis wind turbine
ICC	initial capital cost
LRC	levelized replacement cost
LSS	low speed shaft
NREL	National Renewable Energy Laboratory
NuMAD	Numerical Manufacturing and Design Tool
NWTC	National Wind Technology Center
O&M	operations and maintenance
POD	probability of detection
POMDP	Partially Observed Markov Decision Process
PS	power spectrum
RMS	root mean square
SHPM	structural health prognostics management
SNL	Sandia National Laboratories
SW	shear web
TE	trailing edge
TSA	time synchronous average

EXECUTIVE SUMMARY

Offshore wind energy could potentially play a significant role in helping the U.S. obtain an energy portfolio composed of clean, renewable and diversified resources. One current obstacle to the utilization of offshore wind energy is that most projections put the operations and maintenance (O&M) costs of offshore wind farms between 2 to 5 times the current average O&M costs for onshore wind farms [1]. One way in which those costs may be reduced is through the use of a simple yet effective structural health monitoring system as part of an overall condition based maintenance paradigm. A successful health monitoring system would be able to prevent catastrophic failures, reduce or eliminate unplanned or unnecessary maintenance, and as well reduce logistic lead times and optimize supply chain management through the use of prognostics. In addition to the use of prognostics management for maintenance process improvement, potential exists to also use prognostics to increase energy capture through smart loads management; for example, by derating the turbine so that damage growth is mitigated while revenue production continues until maintenance can be performed.

A methodology has been created to aid in the development, evaluation, and optimization of a structural health and prognostics management (SHPM) system for wind turbines using physics-based simulations and state-space cost modeling. The developed scheme is a multi-scale modeling and simulation approach [16] that propagates the effects of damage from high fidelity local simulations to full turbine simulations using reduced order models as illustrated in Figure 1. Fault and damage detection algorithms have been developed which provide information that feeds into a cost model to compare the cost of energy (COE) between a wind farm that would use a SHPM system to optimize the maintenance schedule and a wind farm which would not use such a system. Figure 2 shows the overall approach to utilizing SHM for optimizing O&M costs.

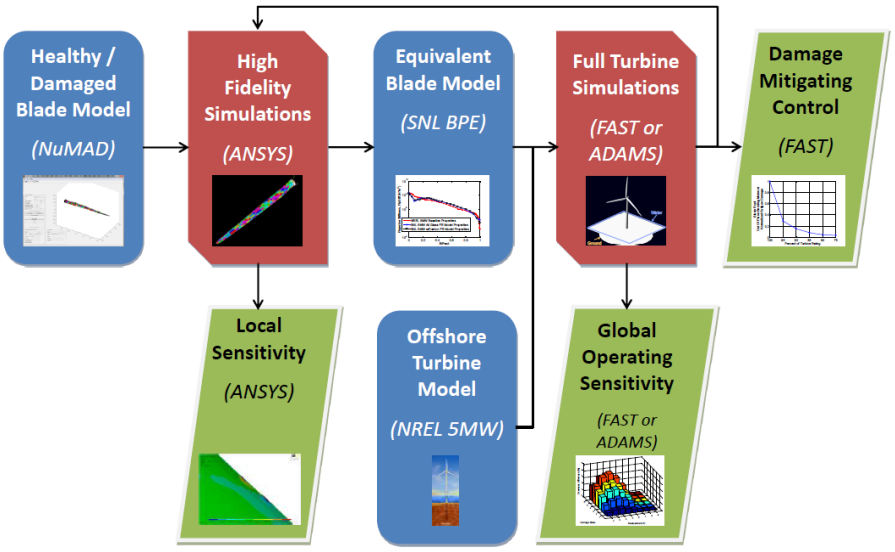

Figure 1. The multi-scale damage modeling and simulation methodology designed to aid in the development and optimization of health monitoring systems for wind turbine blades.

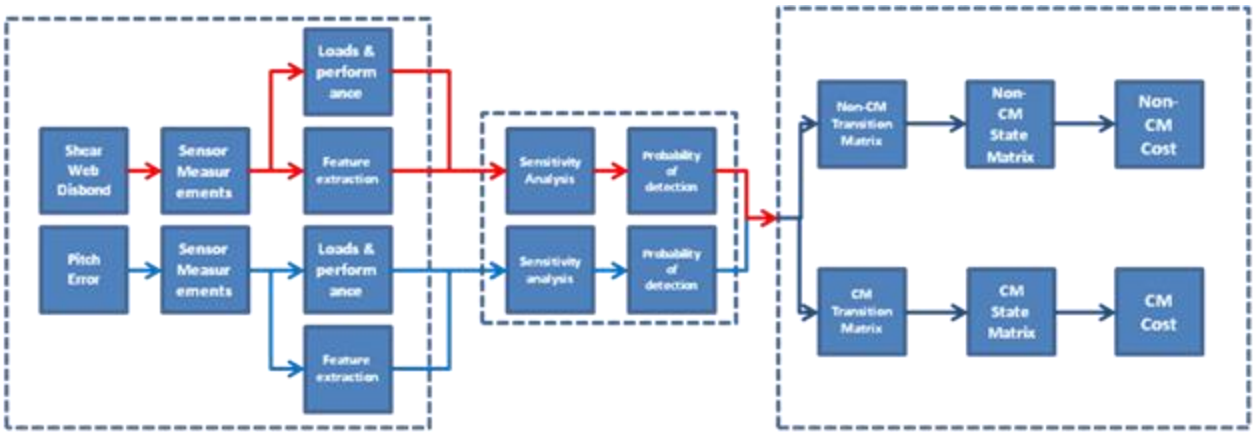

Figure 2. Overall approach for projecting COE benefits based on damage/fault detection strategies (Left Block: Operational Simulation of Damage (see Figure 1); Middle Block: Damage Sensitivity Analysis and Detection Evaluation; Right Block: Cost Analysis)

To expand on work in FY12 [16] where the multi-scale modeling and simulation methodology was implemented and the process in analyzing the effects of a rotor imbalance and shear web disbond was excercised, the work in FY13 was focused on the detection strategies developed for those faults and their sensitivity to several different inflow conditions. Stiffness analysis of the reduced degree-of-freedom beam model of the blade indicated that the SW disbond resulted in; for example, decreases in the blade's flap-wise and torsional stiffness as shown in Figure 3 (the blade root is at blade station 0 in the plots). In sensitivity analyses of the full turbine aeroelastic model incorporating the simplified blade structural model and a wide range of aerodynamic input parameters, the root mean square (RMS) power signal was a good indicator of a pitch error and the blade axial force differences proved to be a good indicator of a mass imbalance (as shown in Figures 4, 5). In addition, a combination of the RMS transverse nacelle acceleration and synchronously averaged 1p blade root pitching moment measurements were able to identify the presence and severity of a shear web disbond. Because the blade's flap-wise and torsional stiffness have a large decrease in the presence of a shear web disbond, this damage mechanism significantly affects the flap-wise and torsional operational response of the turbine. **The simulations results illustrated the benefit of the multiscale modeling approach for detection of rotor imbalances and shear web disbonds and the usefulness of this multi-scale approach to resolve the effects of damage as they are manifested as localized damage in the blade structure and global signatures in the operational sensor measurements.**

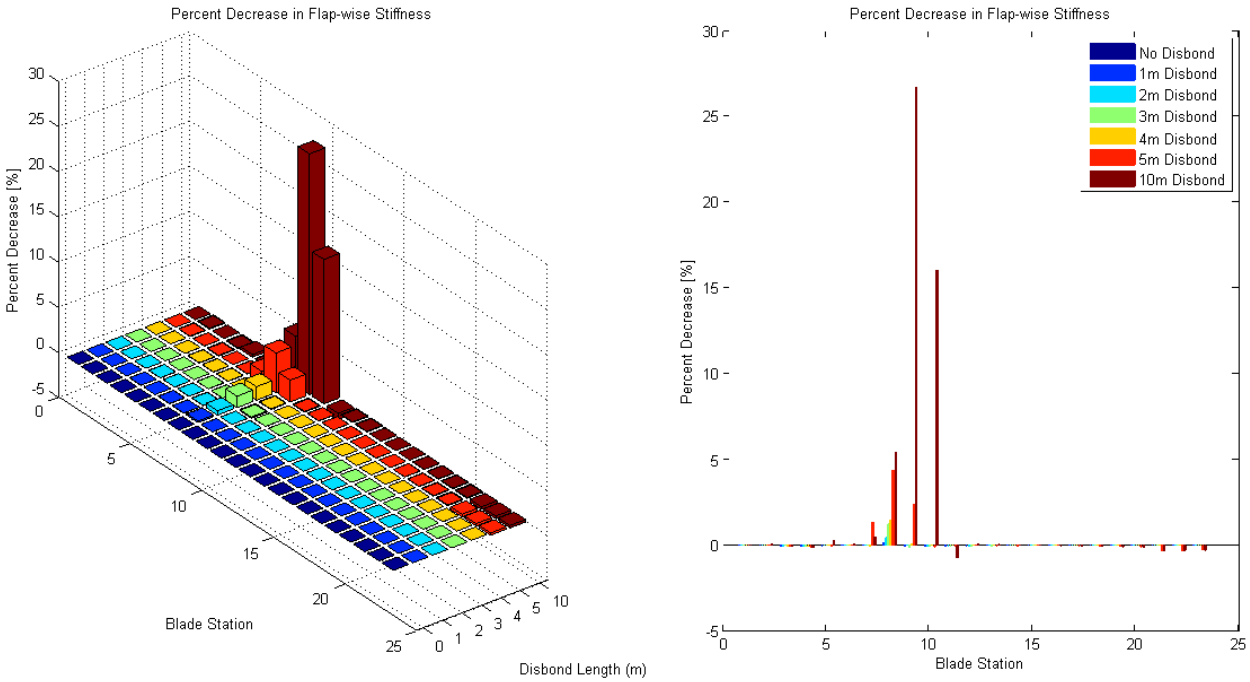

(a)

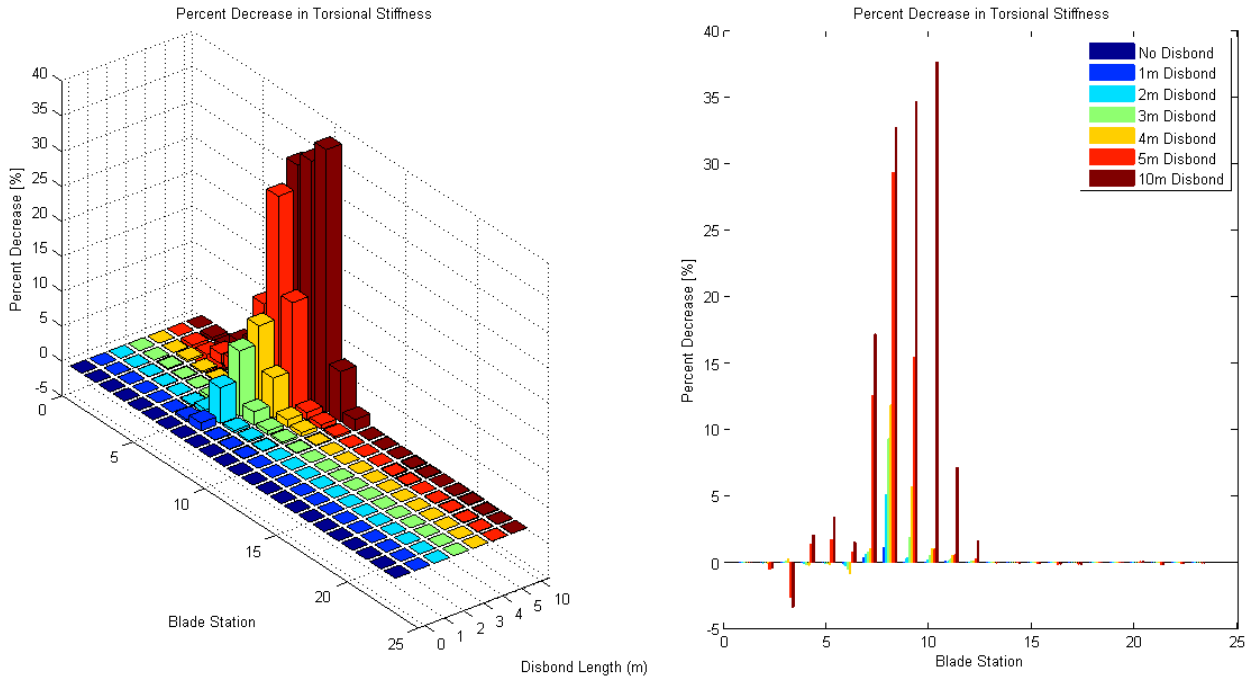

(b)

Figure 3. The percent decreases of the (a) flap-wise stiffness and (b) torsional stiffness values for varying length shear web disbonds along the span of the blade

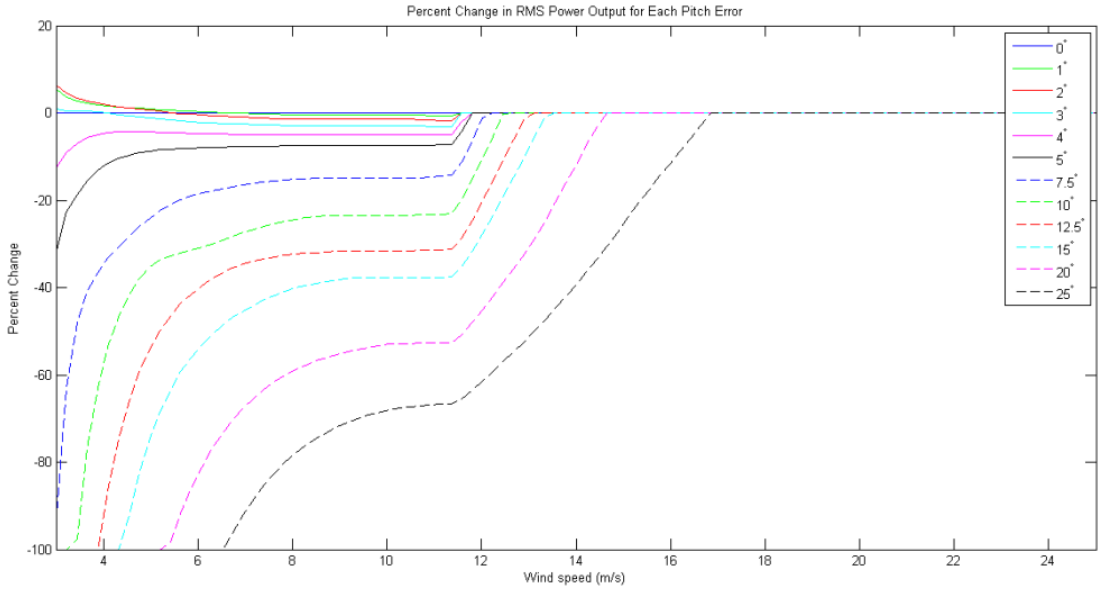

Figure 4. RMS percent change of power output for each pitch error case in varying wind speeds.

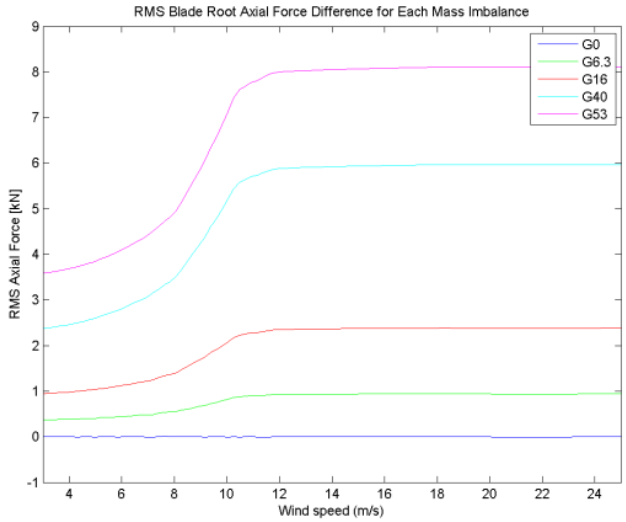

Figure 5. 1p magnitude percent change of edge-wise blade tip acceleration for shear web disbond for four different inflow conditions

A state-based cost model was developed to quantify the effect of a SHPM system on O&M costs. The cost sensitivity analysis shows that the probability of detection of rotor imbalance and shear web disbond increases with the implementation of a SHPM system. In addition, the annual energy production (AEP) increases with the use of a SHPM system. Table 1 shows the POD values of rotor imbalance and shear web disbond, collectively, for SHPM and non-SHPM systems. Figure 6 shows the AEP for SHPM and non-SHPM systems.

Table 1. Weighted Probabilities of detection for SHPM and non-SHPM systems.

Wind Speed	With SHPM	Without SHPM		
	All states	State 2	State 3	State 4
3	21%	5%	10%	16%
6.74	83%	21%	41%	62%
10.48	89%	22%	44%	67%
14.22	92%	23%	46%	69%
17.96	66%	17%	33%	50%
21.7	67%	17%	34%	50%

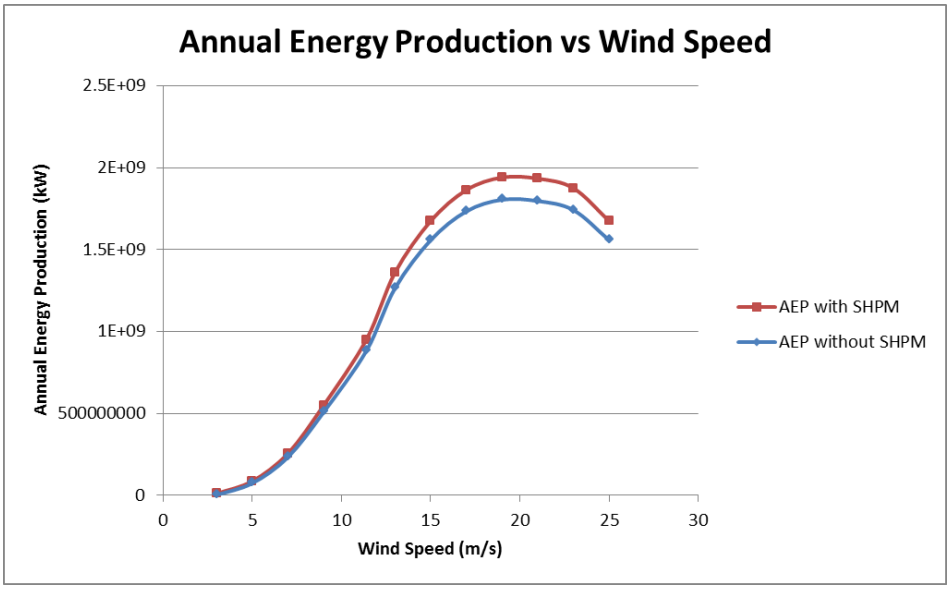

Figure 6. Annual Energy Production versus Wind Speed.

1. INTRODUCTION

Offshore wind energy in the United States is an untapped energy resource that could play a pivotal role in helping the U.S. obtain an energy portfolio composed of clean, renewable and diversified resources. Some of the drivers for the utilization of offshore wind include the proximity of the offshore resources to population centers and the potential for higher capacity factors due to higher resource winds [1]. Because of these drivers and other potential benefits of offshore wind, the Offshore Wind Innovation and Demonstration initiative has developed an ambitious goal of deploying 10 GW of offshore capacity by 2020 at a cost of energy of only $0.10/kWh [2].

1.1. Drivers for Offshore SHPM

As of June 2011, while nine offshore projects totaling over 2 GW of capacity were in various stages of the permitting and development process, no offshore wind energy projects had been installed in the United States [4]. Part of the reason for this lack of development is that operations and maintenance (O&M) costs are expected to be significantly higher for offshore wind turbines than onshore wind turbines. Recent projections of O&M costs have ranged between $11 and $66 U.S. dollars per megawatt-hour with the majority of estimates being between 2 to 5 times the cost of land-based (onshore) O&M [1]. These higher O&M costs represent a larger overall proportion of the cost of energy than for onshore turbines even when the large initial investment required for the installation of offshore turbines is included [5]. One of the reasons that O&M costs are likely to be higher offshore is that the offshore environment will bring with it increased loading which is relatively uncharacterized due to the lack of existing offshore installations. Offshore turbines will also have to be built to withstand the environmental harshness of the offshore environment. Lastly, access to the turbines will be difficult, costly, and occasionally not possible due to high sea states [1,8].

1.2. SHPM Benefits

One potential way in which these O&M costs could be addressed is through the use of a structural health and prognostics management (SHPM) system as part of a condition based maintenance (CBM) paradigm [6-12]. By continuously monitoring the health, or condition, of structural components in each wind turbine, required maintenance actions can be scheduled ahead of time and performed when they are needed rather than on a preset schedule or only after failure has already occurred. The benefits of a CBM strategy are expected to include less regular maintenance, the avoidance or reduction of unscheduled maintenance and improved supply chain management [8-11].

Furthermore, because wind turbines are active systems, monitoring the health of wind turbine components will allow for smart turbine load management to optimize the profit of the entire wind plant. For example, if a turbine blade becomes damaged and that damage is detected at an early stage by the SHPM system, the turbine could be derated so that small less costly repairs could be performed on the turbine. While this action would reduce the amount of power generated by the turbine in the short-term, it may allow for less extensive maintenance actions to be performed, permit additional energy capture while maintenance is being planned, extend the

overall life of the turbine, and allow for multiple turbines to be serviced during the same visit to maximize the overall profit of the wind power plant.

1.3 Summary of Prior Work in Wind Turbine Rotor SHPM Development

Although the fields of structural health monitoring and prognostics management are fairly rich in general, research in application to wind turbine rotor blades in either field is somewhat limited. Integration of the two disciplines is even more limited. Sandia has had an active program for several years to investigate sensored blades with several blade-build and field testing demonstration projects. Blades for utility-scale wind turbines typically have no sensors in the blades and blades with sensors have been limited to strain gauges in the blade root. The Sandia research involved embedding sensors along the entire blade span, which included acceleration, strain, and temperature sensors. The proposed applications for this "enhanced" blade sensing capability include structural health monitoring and active control of the rotor. These Sandia studies provided some important lessons learned regarding manufacturing of sensors into blades and selection of sensors.

In an effort to map out the SHPM problem and also provide an example case study, an initial roadmap was developed by Sandia National Laboratories for combining structural health monitoring and prognostics assets into a SHPM system with application to wind turbine rotor blades as documented in Reference 16. The key element established in this initial roadmap, the so-called multi-scale damage modeling and simulation methodology, addresses both how damage is modeled at multiple resolutions of the model and also the resulting manifestation (or effects) of damage in both the global operating dynamic response and the localized effects related to remaining life (state of health). The intent of this approach is to combine structural health monitoring and prognostic management so as to bridge the gap between being able to detect and characterize the presence of damage and then being able to make revenue-optimizing operations and maintenance decisions.

Reference 17 documents the work performed the following year in which a pilot study consisting of a simulation methodology was carried out to determine the parameters which affect the turbine's operational response in the presence of rotor imbalance and shear web disbond. Preliminary detection strategies were developed for these fault mechanisms and this report provides the results of the sensitivity analyses performed in order to ensure robustness of the detection strategies. The aim of these studies is to provide some additional information to mature the SHPM technology development for wind turbine rotors. The key elements addressed in the report include an assessment of operating sensitivity of damage to damage/fault mechanisms and development/evaluation of an updated O&M cost model.

2. THE APPROACH

In FY12, a multi-model methodology was developed that combines an evaluation of SHPM system performance with state-of-health based cost analysis. The approach permits an evaluation of O&M scenarios (O&M strategies) to identify; for example, turbine conditions strongly influenced by particular fault or damage mechanisms, detection strategies based on various measurement analysis approaches tailored for a wind turbine system, and project operations and maintenance costs with and without such a condition monitoring system. Figure 7 shows the overall approach.

The left-most block in Figure 7 describes modeling of the turbine and damage simulations. The middle block describes the sensitivity analysis performed on the operating response of the turbine including an assessment of sensors and their performance in detecting the modeled damage. The right-most block in Figure 7 describes the cost analysis for the SHPM system. The approach starts with simulations of turbines with damage then the operational response from these simulations is fed to the middle block were the data is analyzed via sensitivity of damage studies. This middle block addresses the performance of the SHPM system to identify which sensors are viable options to detect damage and also to quantify the ability to detect damage (i.e. probability of detection). State of health information and SHPM performance information is fed to the right-most block where SHPM system economics is assessed. This concept should prove useful in assessing both performance and cost of the SHPM system, and in the future it could prove useful in design of the SHPM system and in the evaluation of the return on investment of the SHPM system. This approach could also be applied in real-time operation such that information from the right-most economics module could feedback to the turbine operator or turbine control system for decision making.

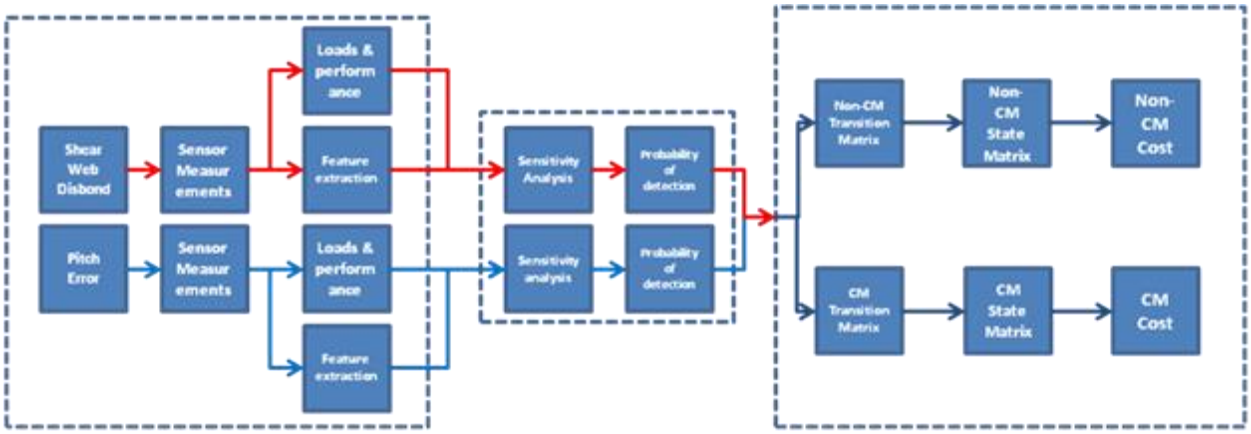

Figure 7. SHPM system feasibility quantification concept approach

The FY13 effort focused on the middle and right blocks. A sensitivity analysis was performed on the rotor imbalance and shear web disbond detection strategies in order to derive probability of detection (POD) values based on the variation of aerodynamic parameters and the extent of damage. In addition, the cost model was revised so that POD values could be used as an input to compare the cost of a wind turbine with and without a SHPM system.

In order to perform the desired simulations, a variety of different software packages were integrated in order to obtain the results of interest. Sandia National Laboratories' (SNL's) NuMAD software was used to create a high fidelity blade model in the software package ANSYS. A shear web disbond was then created in the model and equivalent beam parameters were extracted which could be integrated with a turbine model for simulations of the damaged turbine in either FAST [13] or MSC.ADAMS [14]. Results from each stage of this modeling process were then used to assess the influence of the damage on the response of the blade and the turbine as a whole and to identify a subset of measurements that could prove beneficial for future SHPM investigations.

The cost model used for this study is a state based Excel model that calculates O&M costs of a wind turbine for scenarios such as a turbine with and without an enhanced blade condition monitoring system. Four states are defined in the cost model that correspond to different extents of damage and the associated different types of maintenance that would be required in each state; for example, state 1 is associated with a blade in a new or repaired condition and at the other extreme state 4 would be associated with a blade damaged to the point beyond which it can be repaired and must be replaced.

3. 5-MW OFFSHORE TURBINE MODEL

3.1. Turbine Model Description

As part of an ongoing structural health and prognostics management project for offshore wind turbines, the simulations in this report were performed using a representative utility-scale wind turbine model. The model, known as the NREL offshore 5-MW baseline wind turbine model, was developed by NREL to support studies aimed at assessing offshore wind technology [15]. It is a three-bladed, upwind, variable-speed, variable blade-pitch-to-feather-controlled turbine and was created using available design information from documents published by wind turbine manufacturers, with a focus on the REpower 5-MW turbine. Basic specifications of the model configuration are listed in Table 2.

Table 2. Gross Properties of the NREL 5-MW Baseline Wind Turbine [16].

Property	Value
Rating	5MW
Rotor Orientation, Configuration	Upwind, 3 blades
Control	Variable Speed, Collective Pitch
Drivetrain	High Speed, Multiple-Stage Gearbox
Rotor, Hub Diameter	126 m, 3 m
Hub Height	90 m
Cut-in, Rated, Cut-out Wind Speed	3 m/s, 11.4 m/s, 25 m/s
Cut-in, Rated Rotor Speed	6.9 rpm, 12.1 rpm
Rated Tip Speed	80 m/s
Overhang, Shaft Tilt, Precone	5m, 5°, 2.5°
Rotor Mass, Nacelle Mass, Tower Mass	110,000 kg; 240,000 kg; 347,460 kg
Water Depth	20 m
Wave Model	JONSWAP/Pierson-Moskowitz Spectrum
Significant Wave Height	6 m
Platform	Fixed-Bottom Monopile

A new blade model was developed to be used with the NREL 5-MW turbine model, which is the same model used in the initial studies (Ref). A detailed blade model did not exist and was needed so that damage could be introduced into the blade structure within the multi-scale modeling and simulation framework (as described above). The detailed blade model was developed by Sandia National Laboratories using blade geometry data from the Dutch Offshore Wind Energy Converter Project (DOWEC) and composite layup information from the European Union's UpWind program. The distribution of material layers along the blade span is illustrated in Figure 8.

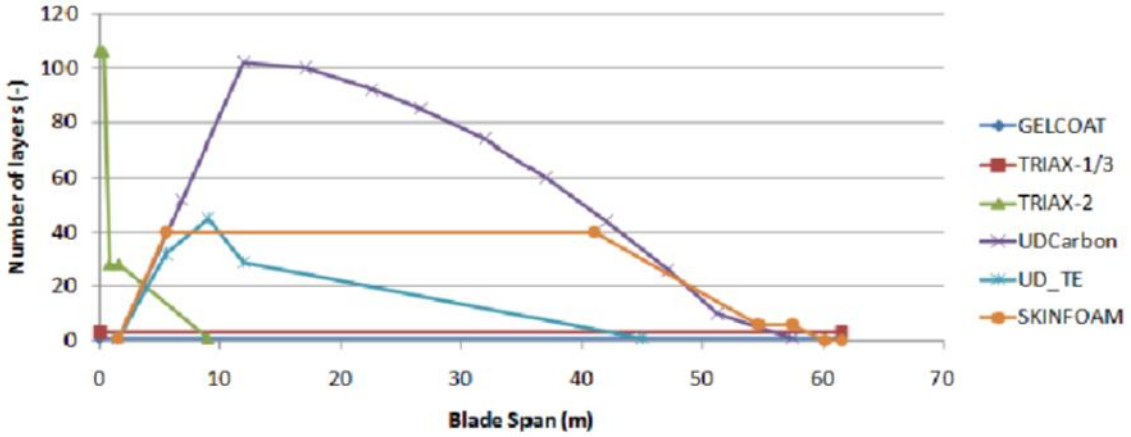

Figure 8. Model of the Distribution of Material Layers along the Span of the Blade, (Griffith, et al. 2011).

Two thirds of the blade span utilizes the TU-Delft family of airfoils, while the final one-third of the blade span utilizes the NACA 64-series airfoils. Intermediate airfoil shapes were developed that preserve the blending of camber lines as well as a smooth blade thickness profile. Figure 9 shows the finite element model of the blade in ANSYS with the colored sections representing different composite materials. This high degree-of-freedom model was translated into a model consisting of several beam elements using Sandia's Blade Property Extraction tool (BPE). BPE works by applying loads in each of the six degrees of freedom at the tip of the blade model in ANSYS, then processing the resulting displacements at selected nodes along the blade to generate the 6x6 Timoshenko stiffness matrices for the beam discretization. This reduced degree-of-freedom model is subsequently used to define the blade properties in FAST. For a more detailed description of BPE, see [16].

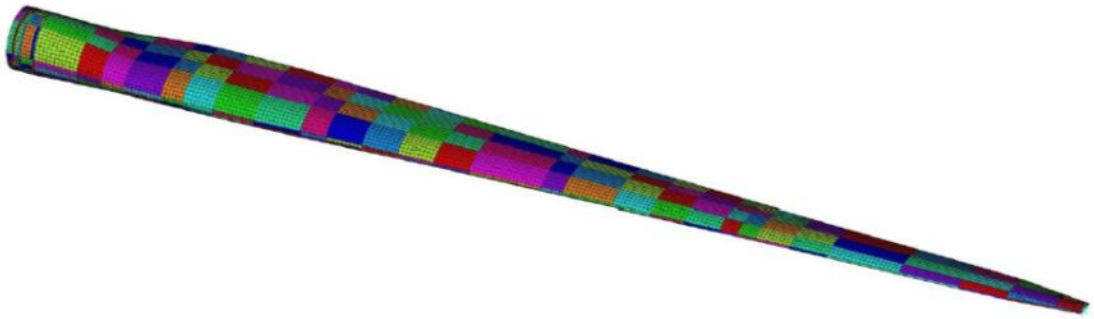

Figure 9. ANSYS finite element mesh for the 5-MW blade model.

3.1.1. *FAST Simulation Turbine Coordinate Systems*

FAST uses six coordinate systems for input and output parameters. Some of these coordinate systems will be referred to throughout this report, so they are reproduced here from the FAST User's Guide for convenience. Note that the FAST User's Guide coordinate system images use a downwind turbine configuration; however, the same coordinate systems apply in the case of the upwind turbine being referred to in this work, but the orientation of the x axis changes so that in either configuration it is pointing in the nominally downwind direction. The rotor shaft

coordinate system is shown in Figure 10. This coordinate system does not rotate with the rotor, but it translates and rotates with the tower and yaws with the nacelle. In addition to output variables related to the low speed shaft, the nacelle inertial measurements also use this coordinate system. Some shaft outputs, such as shear force in the low speed shaft, are measured in both a non-rotating coordinate system and a rotating coordinate system; these are differentiated by using an "s" or "a" subscript, respectively. The tower base coordinate system shown in Figure 11 is fixed in the support platform, thus rotating and translating with the platform. The tower-top/base-plate coordinate system shown in Figure 12 is fixed to the top of the tower. It translates and rotates with the motion of the platform and tower top, but it does not yaw with the nacelle.

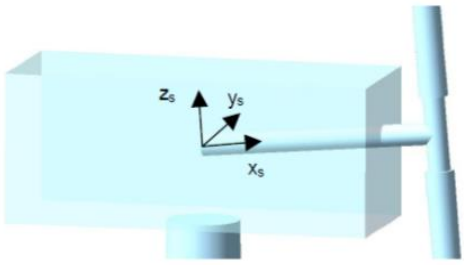

Figure 10. Shaft Coordinate System (Jonkman and Buhl 2005).

Figure 11. Tower Base Coordinate System (Jonkman and Buhl 2005).

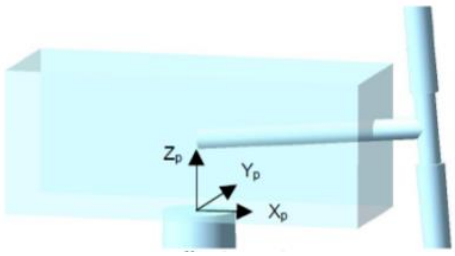

Figure 12. Tower-top/base-plate coordinate system (Jonkman and Buhl 2005).

4. ROTOR MASS/AERODYNAMIC IMBALANCE SENSITIVITY STUDY

4.1. Introduction

A comprehensive aerodynamic uncertainty analysis was conducted to evaluate the detection strategies developed using operational measurements as features to assert the presence and severity of a pitch error or a mass imbalance. Although simultaneous pitch error and mass imbalance was investigated in the pilot study, this sensitivity analysis focuses on solely detecting either a pitch error or mass imbalance. 11,312 FAST simulations were performed to evaluate the robustness of the pitch error and mass imbalance detection strategies and examine their sensitivity to varying parameters including wind speed, horizontal shear, turbulence, and imbalance severity. All of the damage cases for both types of imbalance were applied the same way as in the pilot study. This section includes a variety of different sensitivity analyses that were conducted at various stages throughout the modeling and simulation processes.

4.2. Sensitivity Analysis Methods and Parameters

For this sensitivity analysis, the parameters which were varied include the extent of damage and inflow conditions for the turbine. The NREL offshore 5-MW baseline wind turbine model and FAST were used to simulate the varying parameters. Table 3 shows the matrix of FAST simulations performed for the sensitivity analysis. Operational measurements were analyzed for a healthy turbine in addition to turbines with one of the three blades having a certain level of pitch error or mass imbalance. Mean wind speed, horizontal shear, and turbulence were among the aerodynamic parameters used in this study. For all of the wind profiles, a 1/7 power law vertical shear profile was applied. For all wind profiles, the wind speed was varied from 3 m/s to 25 m/s in 0.22 m/s increments (totaling 101 simulations per turbine damage type). Horizontal shear parameters of 0.3, 0.6, and 0.9 (or 30%, 60%, and 90% horizontal shear) were used (totaling 303 simulations per turbine damage type). The horizontal wind shear parameter is expressed as a linear spectrum of wind speed across the rotor disc. The horizontal wind shear parameter is ranged between -1 and 1, and it represents the wind speed at the blade tip on one side of the rotor minus the wind speed at the blade tip on the opposite side of the rotor, divided by the hub-height wind speed. The horizontal shear is measured in the direction perpendicular to the normally prevailing wind vector. The turbulence models used include the IEC Kaimal Model with A turbulence, the IEC Kaimal Model with B turbulence, and the NREL NWTC wind model with a KHTEST intense disturbance (totaling 303 simulations per turbine damage type).

Table 3. Number of FAST simulations run for each blade imbalance type.

	Pitch Error (0^o, 1^o, 2^o, 3^o, 4^o, 5^o, 7.5^o, 10^o, 15^o, 20^o, 25^o)	**Mass Imbalance (G00, G06, G16, G40, G53)**
Wind Speed (3 – 25 m/s)	**1111**	**505**
Horizontal Shear (30%, 60%, 90%)	**3333**	**1515**
Turbulence (A, B, KHTEST)	**3333**	**1515**

4.3. Analysis of Measurements Used for Detection Strategy

4.3.1. *Pitch Error Analysis Results*

The following sections summarize the trends in the results for pitch error aerodynamic imbalance in the aerodynamic sensitivity study, as measured in the generator power output, nacelle inertial sensors, and low speed shaft bending moments.

4.3.1.1. Generator Power

Since the generator power was used to determine a blade pitch error in the pilot study, this parameter was once again analyzed in order to determine if it can be used for the refined rotor imbalance detection strategy. The rotor azimuth position output from FAST was used as the reference signal for time synchronous averaging. The rotational resampling was performed in the same way as described in the pilot study. The azimuth signal was converted to radians, unwrapped and then the measurement signal was interpolated so that each revolution contained the same number of data samples with each sample corresponding to the same azimuth position of the rotor's rotation. Three revolutions of data blocks were averaged together. By using more than one revolution in the block size, the length of the block's time history could be increased which in turn increases the frequency resolution of the DFT of the time-averaged signal.

As expected, the generator power decreased in the presence of increasing pitch errors when varying the wind speed, horizontal shear, and turbulence wind profiles. As the wind speed increases beyond the turbine's rated speed of 11.4 m/s, the generator power for the damage cases converge with the healthy case. In addition, the wind speed at which the generator power for damage and healthy cases converge increases as the amount of pitch error is also increased. These results reinforce the importance of detecting an aerodynamic imbalance before it becomes severe. Figures 13 and 14 show the RMS power and percent change in power output for the laminar wind profile in the presence of a pitch error.

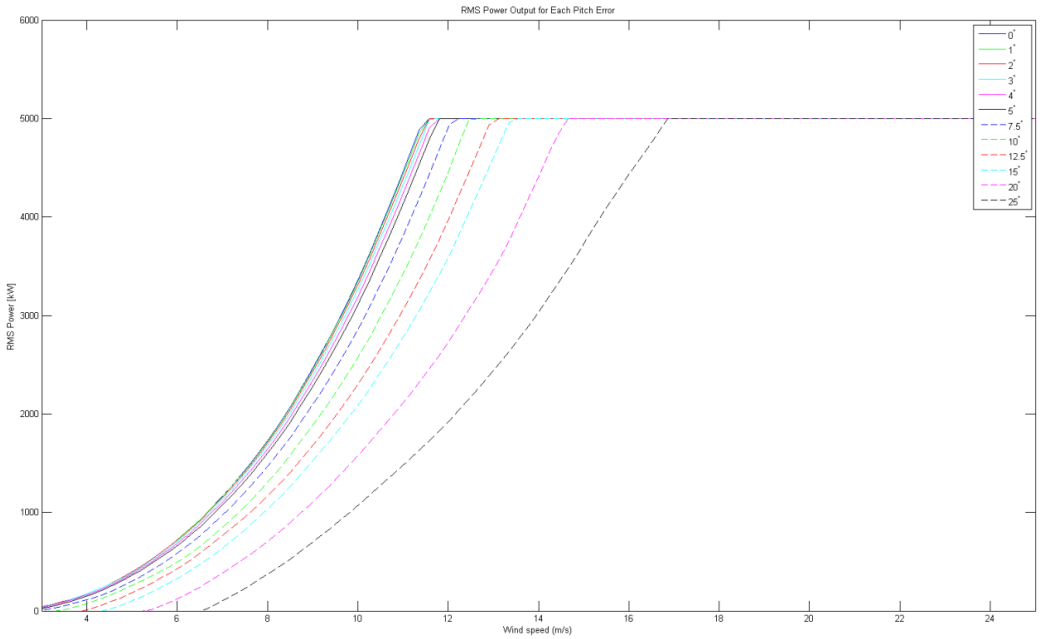

Figure 13. RMS power output for each pitch error case in varying wind speeds.

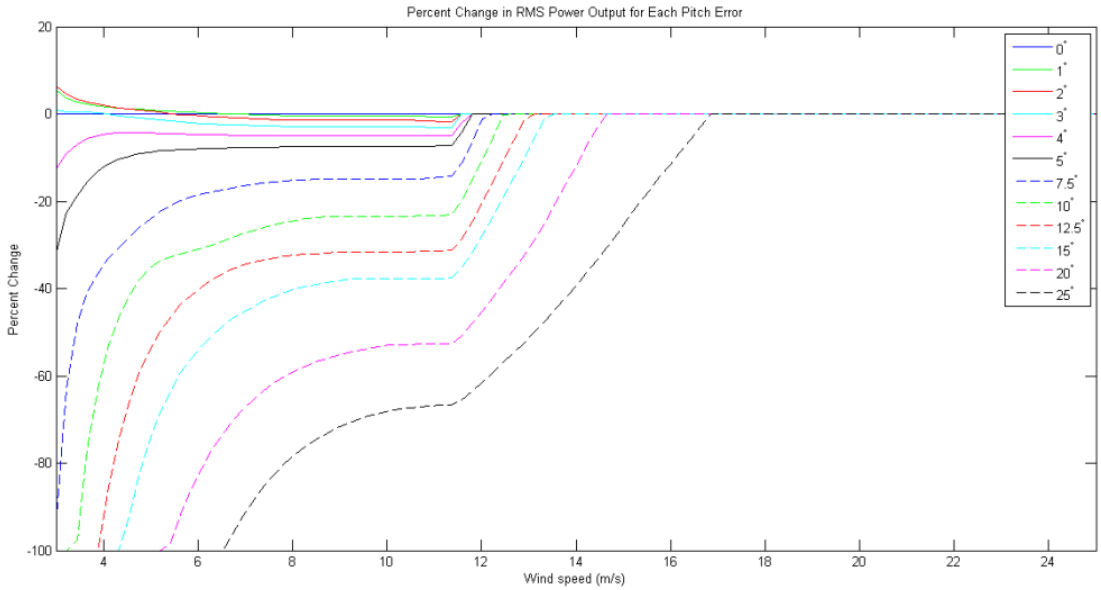

Figure 14. RMS percent change of power output for each pitch error case in varying wind speeds.

4.3.1.2. Low Speed Shaft Bending Moment

The low speed shaft (LSS) bending moment also displayed significant changes due to pitch error. Figure 15 shows the RMS rotating LSS bending moment for each pitch error case. As was seen in the RMS power output, the RMS LSS bending moment decreased as the pitch error increased for wind speeds up to 16.86 m/s. Since the generator power can be subject to electrical faults, measurements of the LSS torque may be a better feature choice, especially since it shares the same trends as the RMS power output.

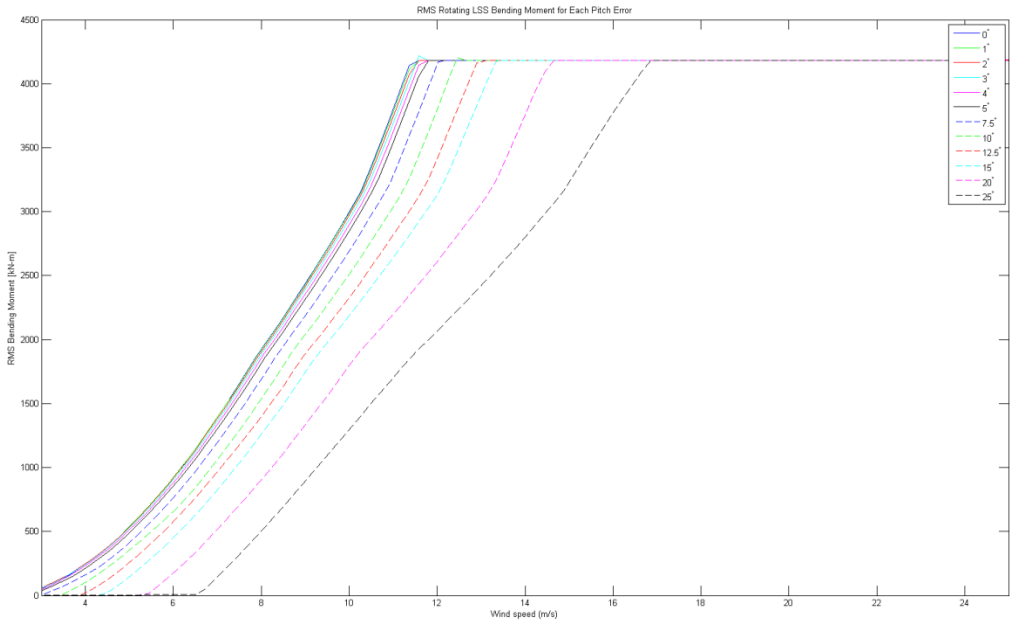

Figure 15. RMS low speed shaft bending moment for each pitch error case in varying wind speeds.

4.3.2. *Mass Imbalance Analysis Results*

The following sections summarize the trends in the results for mass imbalance in the aerodynamic sensitivity study, as measured in the same non-blade measurements of generator power output and low speed shaft bending moment.

4.3.2.1. Generator Power

Figure 16 shows the percent change in RMS power output under several mass imbalance cases. The figure indicates that the RMS power output remained unchanged in the presence of five different levels of mass imbalance: G0 (baseline, no imbalance), G6.3, G16, G40, and G53 (representing the 0.5% total blade mass imbalance). Since only pitch error affects the RMS power output, this would serve as a good indicator of an aerodynamic imbalance.

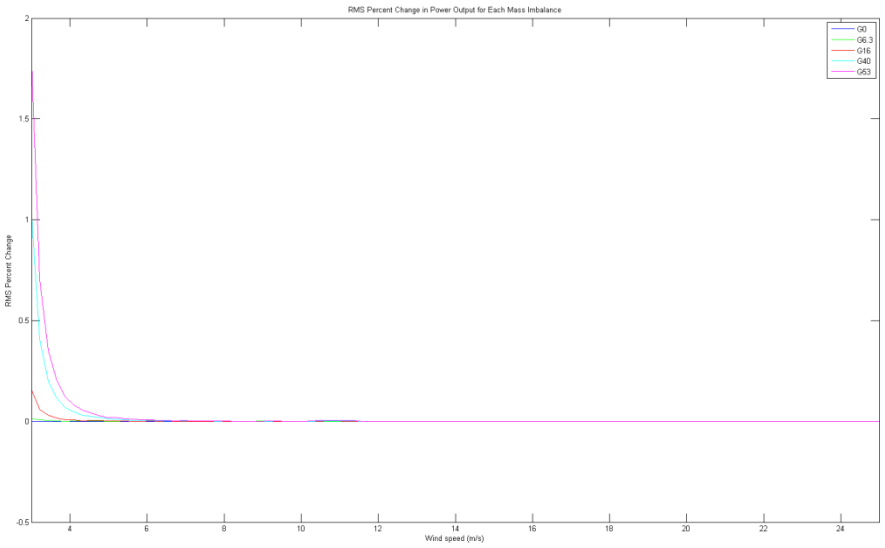

Figure 16. Percent change in RMS power output for each mass imbalance case in varying wind speeds.

4.3.2.2. Blade Root Axial Force

The blade root axial force was used to determine a blade mass imbalance in the pilot study, so this parameter was again analyzed in order to determine if it can be used for the refined rotor imbalance detection strategy. The time synchronous averaging and rotational resampling were performed the same way as described in Section 4.3.1.1.

The blade root axial force again increased in the presence of increasing mass imbalances for all wind profiles. Up to the rated speed of the turbine, the RMS axial force diverged with wind speed as the mass imbalance increased. After the turbine reaches its rated speed, the blade root axial force differences remain constant. Figures 17 and 18 show the RMS blade root axial force differences for the laminar and A turbulence wind profiles in the presence of a mass imbalance.

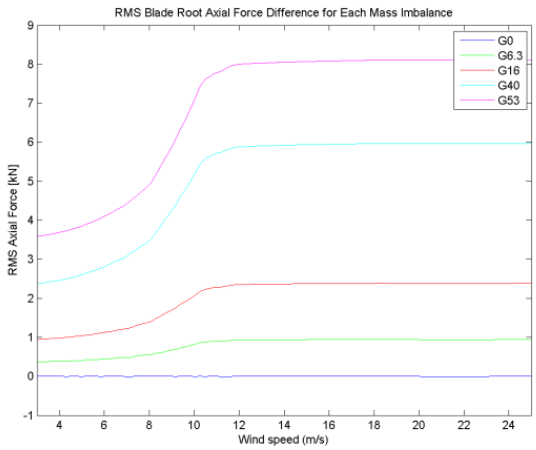

Figure 17. RMS blade root axial force for mass imbalance in varying wind speeds.

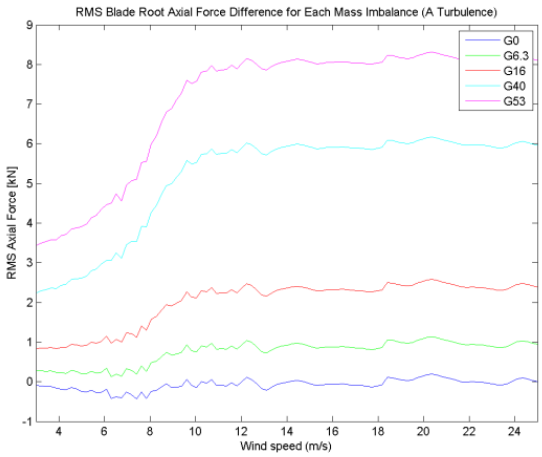

Figure 18. RMS blade root axial force for mass imbalance in A turbulence.

4.4. Summary of Imbalance Detection Strategy Refinements

The results of the sensitivity analysis and key measurements have been used to refine a rotor imbalance detection strategy. This strategy employs both blade and non-blade sensor measurements. Specifically, non-blade sensor measurements are used as the indicator for a pitch error and the blade sensors (strain gages at the blade root to measure the axial force) are used to detect a mass imbalance and its level of severity. The action strategy and flow chart have not changed; however, each rotor imbalance has been assigned thresholds corresponding to the severity of the imbalance, as shown below in Tables 4 and 5 for pitch error and mass imbalance, respectively.

Table 4. Pitch error damage state and corresponding feature used for classification

State 1 (Healthy, 0^o pitch error)	Measured RMS power >= expected healthy RMS power
State 2 (2^o, 3^o, 4^o, 5^o pitch errors)	Greater than zero and less than 10% decrease in measured RMS power
State 3 (7.5^o, 10^o, 12.5^o, 15^o pitch errors)	Greater than 10% and less than 51% decrease in measured RMS power
State 4 (20^o, 25^o, and higher pitch errors)	Greater than 51% decrease in measured RMS power

Table 5. Mass imbalance damage state and corresponding feature used for classification

State 1 (Healthy, no mass imbalance)	Measured blade axial force difference >= 300 N increase in expected healthy blade axial force difference
State 2 (G6.3 mass imbalance)	Greater than or equal to 300 N and less than 950 N increase in measured blade axial force difference
State 3 (G16 mass imbalance)	Greater than 950 N and less than 2300 N increase in measured blade axial force difference
State 4 (G40, G53, and higher mass imbalances)	Greater than 2300 N increase in measured blade axial force difference

Probability of detection values were calculated for detecting the presence of a pitch error or mass imbalance in addition to detecting three different damage states which vary by severity. See

Tables 4 and 5 for the damage state classifications of pitch error and mass imbalance, respectively. These damage state classifications were used for each FAST simulation and inflow condition. **If the measurement at a given wind speed, profile, and damage state met the criteria described in the tables above, then it was deemed a success. Otherwise, it was deemed a failure.** For example, the blade root axial force is extracted from the simulation for the 3.88 m/s laminar wind profile and for a turbine with a blade which has a G16 mass imbalance. If the blade root axial force difference is greater than 950 N and less than 2300 N, then the detection is a success and given a "1" value at that data point. If it does not meet the criteria, it is given a "0" value. The number of successes is then added up for each POD category and that total is divided by the total number of simulations in that category (101 simulations for the full wind speed range of 3–25 m/s). The resultant percentage is the probability of detection for that damage state and wind profile. For state 2 through 4, the POD is calculated for the probability that the presence of damage is detected in addition to the classification for that damage class, respectively. Tables 6 and 7 show the POD values for detecting the presence of a pitch error or mass imbalance and then categorizing the damage into each damage case, respectively.

The PODs were calculated over the entire wind speed range in addition to an enhanced wind speed range which optimizes the resulting POD value for accurate damage detection for all wind loading cases. In other words, the measurements, algorithms, and probability of detection calculations are only done within the wind speed range defined in the tables below. The optimized wind speed range and corresponding POD values are highlighted in green in the table. In addition, each POD value was weighted by the Weibull distribution to incorporate the frequency of each wind speed used within the analyzed range. The weighted pitch error POD results show that the developed algorithms are at least 96.28% successful for all of the FAST simulations except the turbulence cases for damage states 3 and 4. Since the weighted success rate of detecting the presence of a pitch error is 96.28% or higher, those pitch errors which fail to be classified in states 3 and 4 in turbulent conditions will still be detected as being in a damaged state. If the algorithm is unable to classify the pitch error severity, then another measurement will be made as soon as the inflow is no longer turbulent. Inflow characteristics can be defined with an ultrasonic anemometer in order to determine the wind profile. As for mass imbalance, its PODs were 100% successful in the optimized wind speed range for all wind profiles.

Table 6. Probabilities of detection for pitch error

		PRESENCE OF DAMAGE		STATE 2 (2, 3, 4, 5 deg error)		STATE 3 (7.5, 10, 12.5, 15 deg error)		STATE 4 (20, >= 25 deg error)	
		3 - 25 m/s	6 - 11.4 m/s	3 - 25 m/s	6 - 11.4 m/s	3 - 25 m/s	6 - 11.4 m/s	3 - 25 m/s	6 - 11.4 m/s
LAMINAR	Raw	36.63%	100.00%	34.09%	100.00%	9.07%	96.00%	14.15%	100.00%
	Weibull Weighted	59.12%	100.00%	54.16%	100.00%	25.13%	96.10%	36.52%	100.00%
30% SHEAR	Raw	41.58%	100.00%	38.70%	100.00%	10.29%	96.00%	16.06%	100.00%
	Weibull Weighted	64.99%	100.00%	59.54%	100.00%	27.62%	96.10%	40.14%	100.00%
60% SHEAR	Raw	39.60%	100.00%	36.86%	100.00%	9.41%	96.00%	15.29%	100.00%
	Weibull Weighted	63.36%	100.00%	58.05%	100.00%	25.98%	96.10%	39.13%	100.00%
90% SHEAR	Raw	36.63%	50.00%	33.73%	96.00%	9.07%	96.00%	14.15%	96.00%
	Weibull Weighted	60.05%	96.41%	54.17%	96.41%	25.62%	96.41%	37.09%	96.41%
A TURBULENCE	Raw	92.08%	96.00%	87.52%	96.00%	17.32%	61.44%	22.79%	42.24%
	Weibull Weighted	89.97%	96.28%	84.84%	96.28%	29.50%	63.11%	34.44%	43.28%
B TURBULENCE	Raw	94.06%	100.00%	89.40%	100.00%	18.63%	64.00%	23.28%	44.00%
	Weibull Weighted	93.30%	100.00%	87.97%	100.00%	32.02%	65.55%	35.71%	44.95%
KHTEST TURBULENCE	Raw	36.63%	100.00%	34.82%	100.00%	6.17%	52.00%	8.71%	40.00%
	Weibull Weighted	60.48%	100.00%	57.03%	100.00%	17.59%	53.26%	22.07%	40.78%

Table 7. Probabilities of detection for mass imbalance

		PRESENCE OF DAMAGE		STATE 2 (G6.3 IMBALANCE)		STATE 3 (G16 IMBALANCE)		STATE 4 (G40, >= G53 IMBALANCE)	
		3 - 25 m/s	11.4 - 25 m/s	3 - 25 m/s	11.4 - 25 m/s	3 - 25 m/s	11.4 - 25 m/s	3 - 25 m/s	11.4 - 25 m/s
LAMINAR	Raw	100.00%	100.00%	99.01%	100.00%	99.01%	100.00%	100.00%	100.00%
	Weibull Weighted	100.00%	100.00%	98.98%	100.00%	98.98%	100.00%	100.00%	100.00%
30% SHEAR	Raw	100.00%	100.00%	99.01%	100.00%	99.01%	100.00%	100.00%	100.00%
	Weibull Weighted	100.00%	100.00%	98.98%	100.00%	98.98%	100.00%	100.00%	100.00%
60% SHEAR	Raw	100.00%	100.00%	100.00%	100.00%	100.00%	100.00%	100.00%	100.00%
	Weibull Weighted	100.00%	100.00%	100.00%	100.00%	100.00%	100.00%	100.00%	100.00%
90% SHEAR	Raw	100.00%	100.00%	100.00%	100.00%	100.00%	100.00%	100.00%	100.00%
	Weibull Weighted	100.00%	100.00%	100.00%	100.00%	100.00%	100.00%	100.00%	100.00%
A TURBULENCE	Raw	80.20%	100.00%	71.46%	100.00%	71.46%	100.00%	78.61%	100.00%
	Weibull Weighted	70.46%	100.00%	60.40%	100.00%	60.40%	100.00%	68.98%	100.00%
B TURBULENCE	Raw	80.20%	100.00%	71.46%	100.00%	71.46%	100.00%	79.40%	100.00%
	Weibull Weighted	70.52%	100.00%	60.40%	100.00%	60.40%	100.00%	69.80%	100.00%
KHTEST TURBULENCE	Raw	85.15%	100.00%	79.25%	100.00%	79.25%	100.00%	84.31%	100.00%
	Weibull Weighted	78.83%	100.00%	72.19%	100.00%	72.19%	100.00%	78.03%	100.00%

5. SHEAR WEB DISBOND SENSITIVITY STUDY

5.1. Introduction

A comprehensive aerodynamic uncertainty analysis was also conducted to evaluate the detection strategy developed using operational measurements as features to assert the presence and severity of a shear web disbond (as described in the FY12 report). 4,949 FAST simulations were performed to evaluate the robustness of the shear web disbond detection strategy and examine its sensitivity to varying parameters including wind speed, horizontal shear, turbulence, and disbond length. All of the disbonds were assumed to have initiated at max chord of the blade (at the 14.35 meter span location) and propagated outwards toward the tip of the blade. This section includes a variety of different sensitivity analyses that were conducted at various stages throughout the modeling and simulation processes.

5.2. Sensitivity Analysis Methods and Parameters

For this sensitivity analysis, the parameters which were varied include the extent of damage and inflow conditions for the turbine. The NREL offshore 5-MW baseline wind turbine model and FAST were used to simulate the varying parameters. Table 8 shows the matrix of FAST simulations performed for the sensitivity analysis. Operational measurements were analyzed for a healthy turbine in addition to turbines with one of the three blades containing a shear web disbond of 1, 2, 3, 4, 5, or 10 meters in length. Mean wind speed, horizontal shear, and turbulence were among the aerodynamic parameters used in this study. The wind profiles were defined as described for the rotor imbalance sensitivity analysis in Section 4.

Table 8. Number of FAST simulations performed for each blade damage type.

	Healthy	1m Disbond	2m Disbond	3m Disbond	4m Disbond	5m Disbond	10m Disbond
Wind Speed (3 – 25 m/s)	101	101	101	101	101	101	101
Horizontal Shear (30%, 60%, 90%)	303	303	303	303	303	303	303
Turbulence (A, B, KHTEST)	303	303	303	303	303	303	303

5.3. Shear Web Disbond Sensitivity and Structural Effects

The shear web disbond damage cases were expanded to include disbond lengths of 1, 2, 3, 4, 5, and 10 meters. The stiffness values of each blade damage case were extracted from each section of their reduced order models. Figures 19-22 show the percent decreases in edge-wise, flap-wise, torsional, and axial stiffness, respectively. As expected, all four stiffness parameters decreased at the damage location as the disbond length was increased. The shear web disbond also greatly affected the blade's torsional stiffness, reiterating that measurements which are sensitive to the blade's torsional response will be good indicators that a shear web disbond is present.

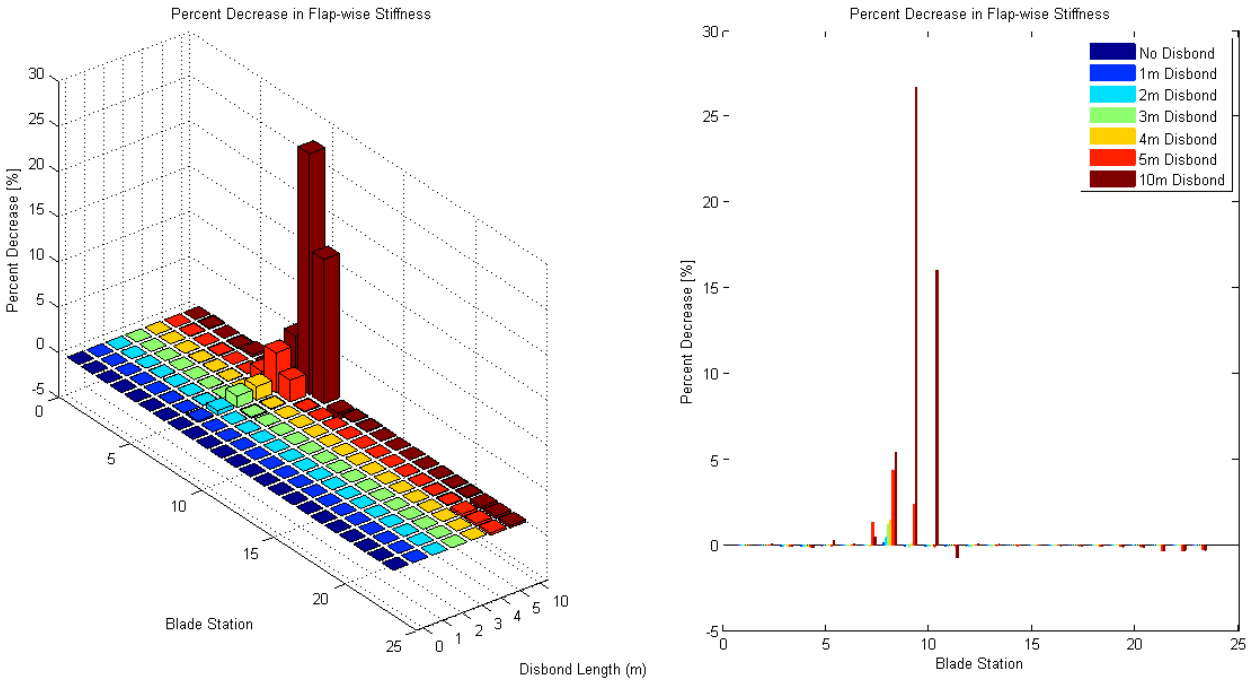

Figure 19. The percent decreases of the flap-wise stiffness value for varying length disbonds for segments spaced along the length of the blade

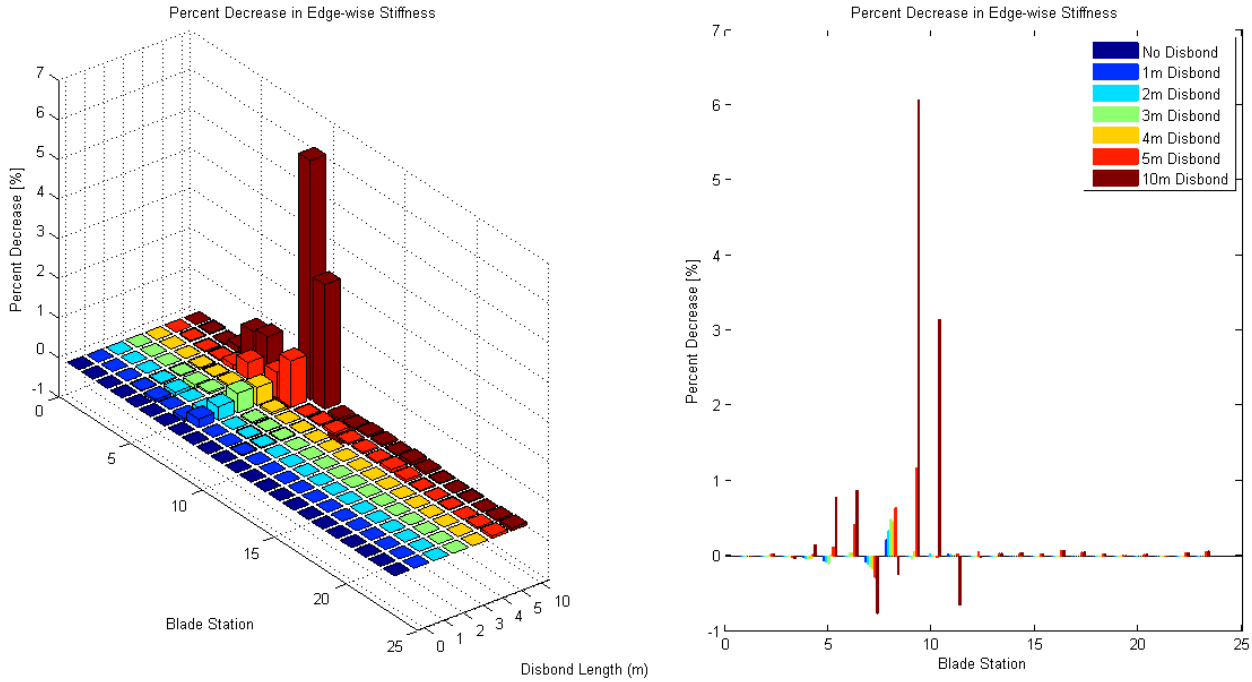

Figure 20. The percent decreases of the edge-wise stiffness value for varying length disbonds for segments spaced along the length of the blade

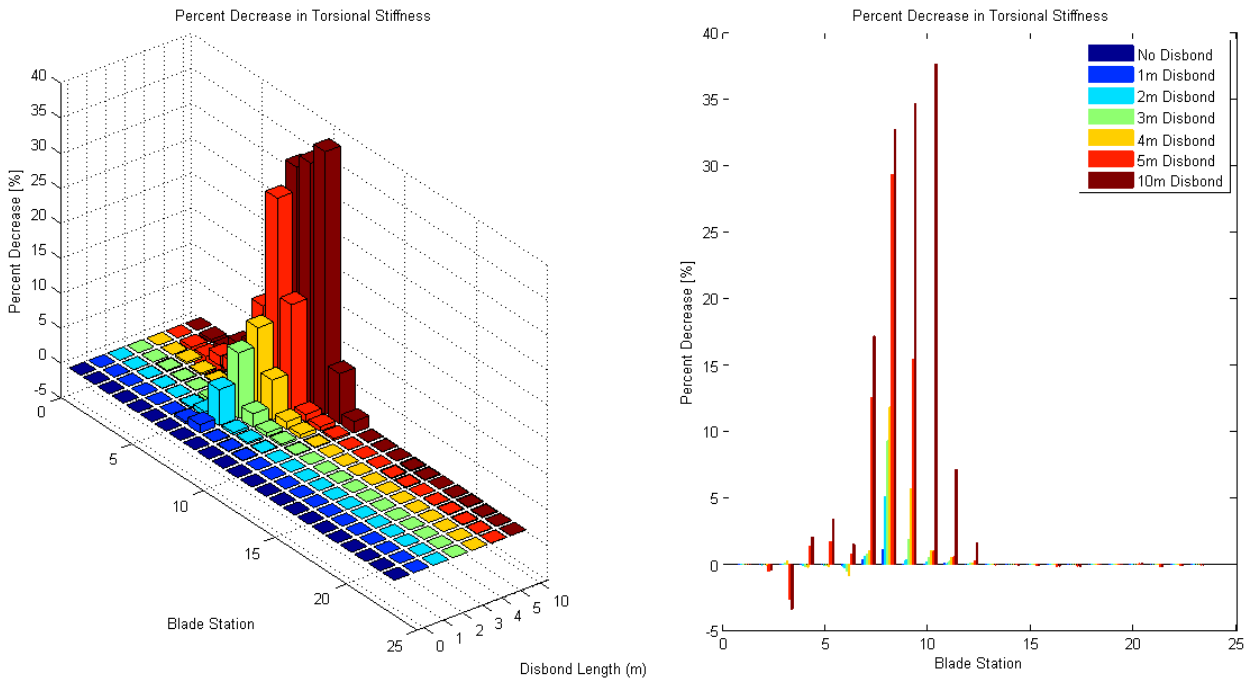

Figure 21. The percent decreases of the torsional stiffness value for varying length disbonds for segments spaced along the length of the blade

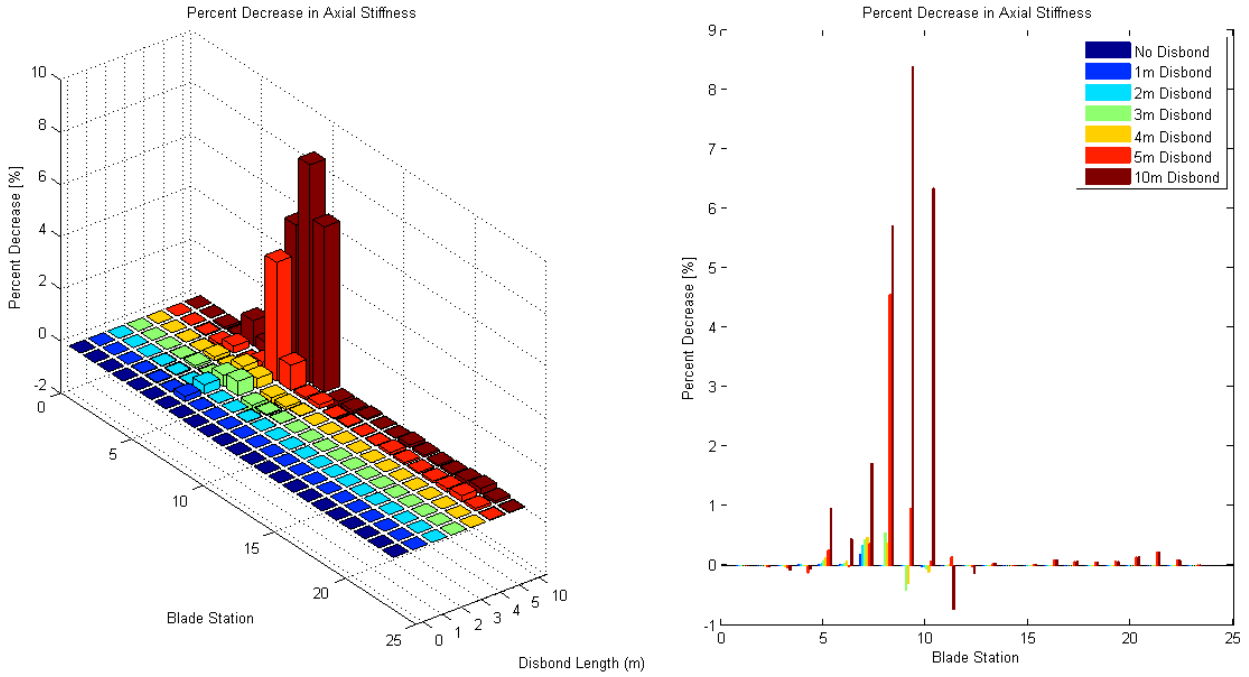

Figure 22. The percent decreases of the axial stiffness value for varying length disbonds for segments spaced along the length of the blade

5.4. Analysis of Measurements Used for Detection Strategy

Analysis was once again applied to blade and non-blade sensors to compare the effectiveness and robustness of the shear web disbond detection strategy described in the FY12 report. All measurements outlined in FY12 were examined to determine if any non-bladed sensors could be used for a refined detection strategy. From the variables analyzed from the FAST simulation outputs, those which displayed significant percentage changes in their RMS value or frequency response magnitude at the operating speed given a blade shear web disbond were identified as key measurement channels. The rotor azimuth position output from FAST was used as the reference signal for time synchronous averaging. The rotational resampling was performed in the same way as described in the FY12 report. The azimuth signal was converted to radians, unwrapped and then the measurement signal was interpolated so that each revolution contained the same number of data samples with each sample corresponding to the same azimuth position of the rotor's rotation. Three revolutions of data blocks were averaged together. By using more than one revolution in the block size, the length of the block's time history could be increased which in turn increases the frequency resolution of the DFT of the time-averaged signal. The shear web disbond detection algorithms for the selected measurements all functioned in a similar way: detecting changes from baseline measurements either in the RMS response or 1p power spectral density magnitude.

5.4.1. *Shear Web Disbond Analysis Results*

The following sections summarize the trends in the results for shear web disbond, as measured in the generator power output and magnitude of the nacelle inertial sensors, blade tip inertial sensors, blade root strain sensors, and blade root inertial sensors.

5.4.1.1. Generator Power

Overall, the generator power did not change significantly in the presence of a shear web disbond when varying the wind speed, horizontal shear, and turbulence wind profiles. The power output experienced a few transients between the cut-in and rated speeds during the turbulent simulations, although all of the power output changes after the turbine reached the rated speed were negligible. Figure 23 shows the RMS percent change in power output for the laminar wind profile in the presence of a shear web disbond.

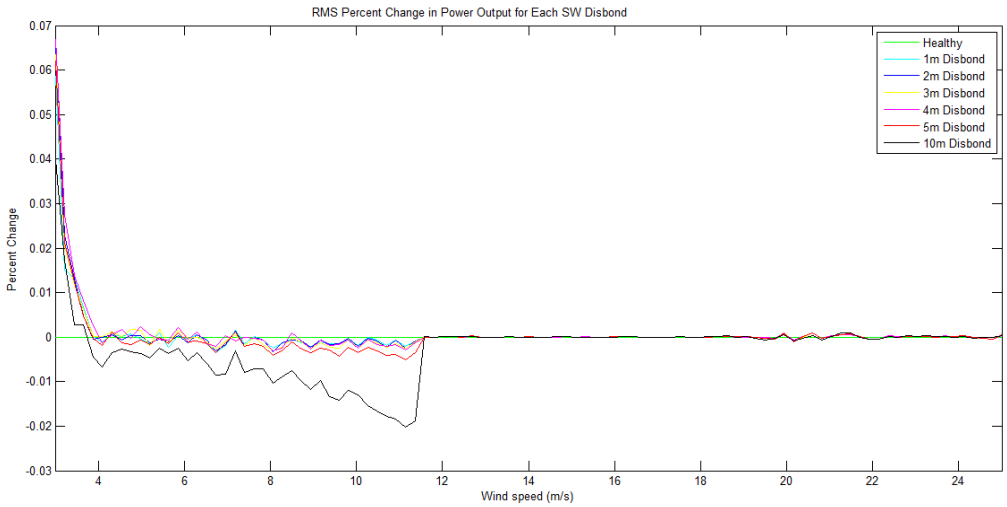

Figure 23. RMS percent change of power output for shear web disbond in varying wind speeds.

5.4.1.2. Nacelle Inertial Measurements

For all wind profiles and damage cases, the RMS value of the nacelle acceleration in all three directions increased at the turbine's rated wind speed (11.4 m/s) or higher. As was seen in the pilot study, the transverse nacelle acceleration showed a clear RMS increase for all aerodynamic cases between the rated speed and approximately 20 m/s (shown in Figure 25). In addition, the nacelle accelerations increased as the shear web disbond length was increased. Figures 24 - 26 show the RMS percent change in nacelle acceleration in the axial, transverse, and vertical directions respectively. The 1p response magnitude was analyzed as well, but the trends of an increasing magnitude were not as apparent for all of the wind loading cases. Because these measurements were made at the nacelle hub, it is not possible to determine the problematic blade if one of the three blades has the shear web disbond. However, these measurements can be used to indicate that a shear web disbond is present and then trigger more sophisticated measurements to be used to determine which blade has the disbond and the severity of the damage.

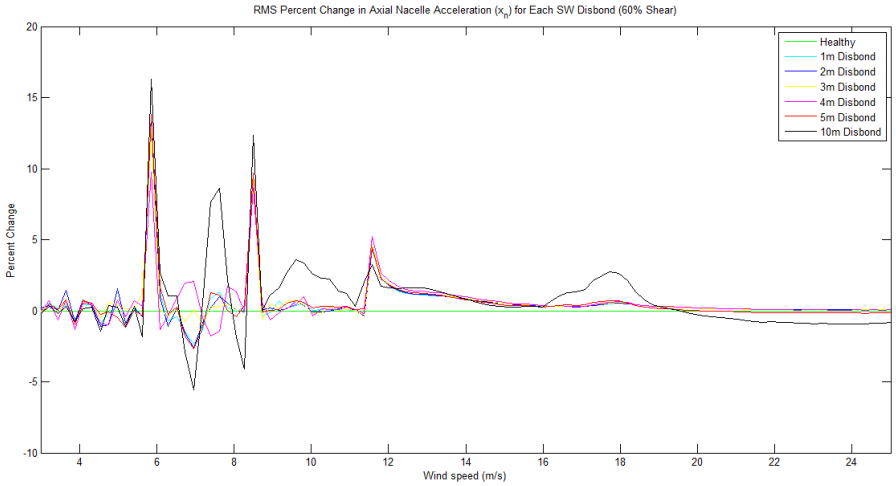

Figure 24. RMS percent change of axial nacelle acceleration for shear web disbond in 60% horizontal shear.

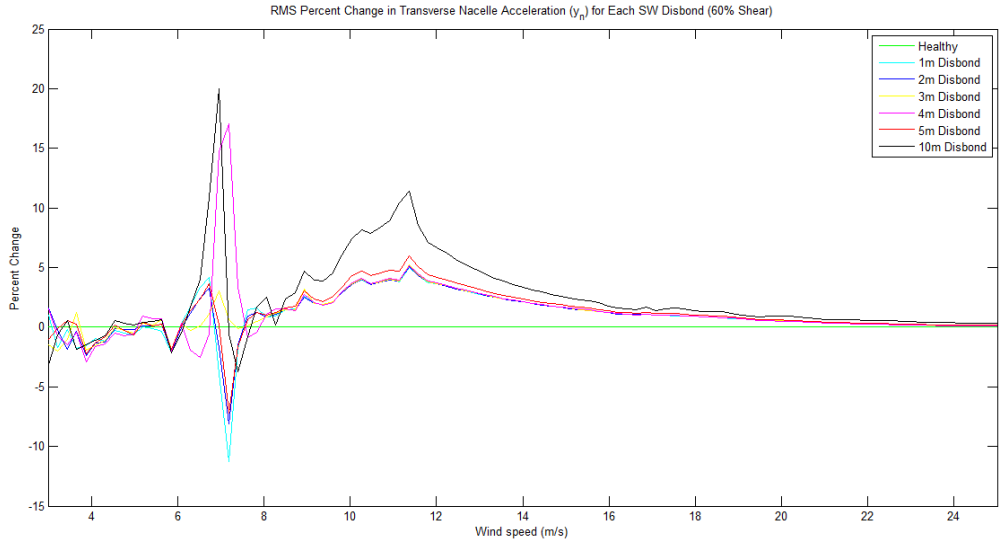

Figure 25. RMS percent change of transverse nacelle acceleration for shear web disbond in 60% horizontal shear.

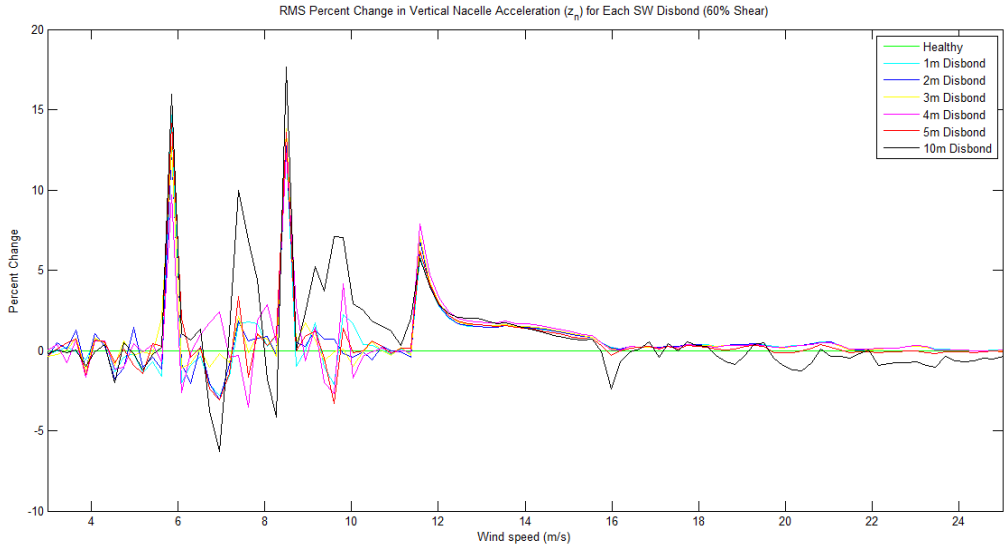

Figure 26. RMS percent change of vertical nacelle acceleration for shear web disbond in 60% horizontal shear.

5.4.1.3. Blade Tip Acceleration Response

The percent change in the RMS response magnitude of the edge-wise blade tip acceleration for shear web disbond at different wind speeds is shown in Figure 27. Although the edge-wise blade tip acceleration was affected by the presence of a shear web disbond, these algorithms did not present a trend that could be correlated to an increase in disbond length.

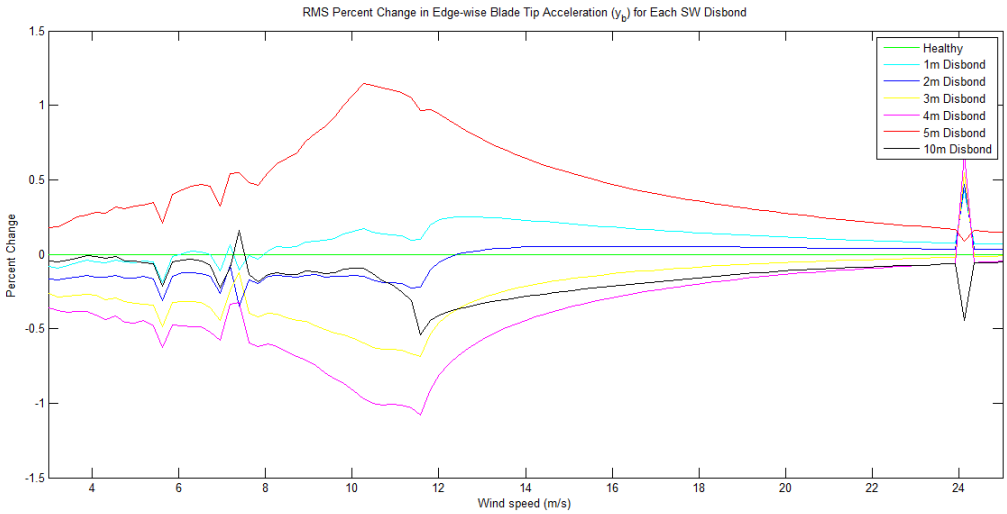

Figure 27. RMS percent change of edge-wise blade tip acceleration for shear web disbond in varying wind speeds.

The span-wise blade tip acceleration 1p response differences are shown in Figures 28 and 29. The plots show that when a shear web disbond was present, the 1p power spectrum response difference was always positive up to 18 m/s for all wind loading cases. Although there doesn't appear to be a trend that shows the severity of the damage, this measurement can serve as a good indicator that a shear web disbond is present.

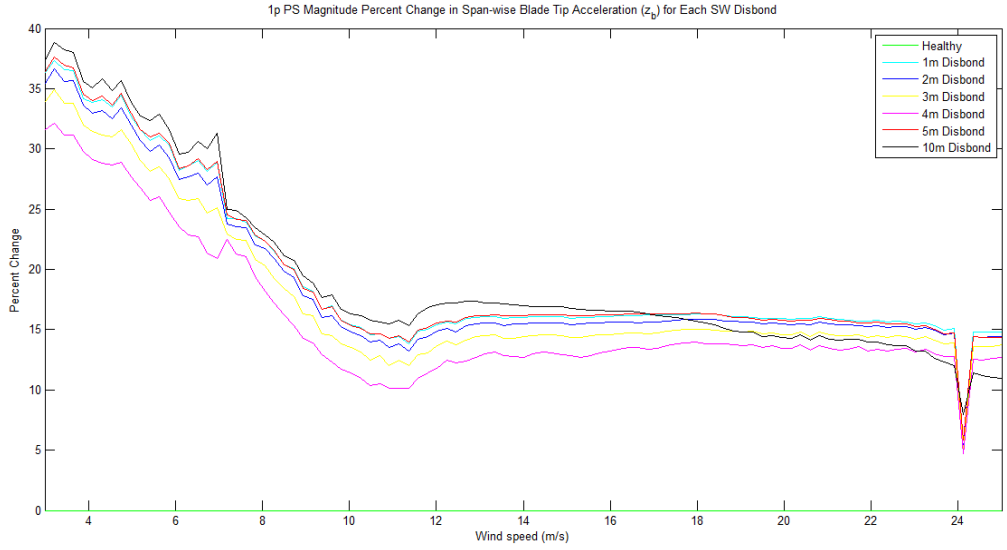

Figure 28. 1p magnitude percent change of span-wise blade tip acceleration for shear web disbond in varying wind speeds.

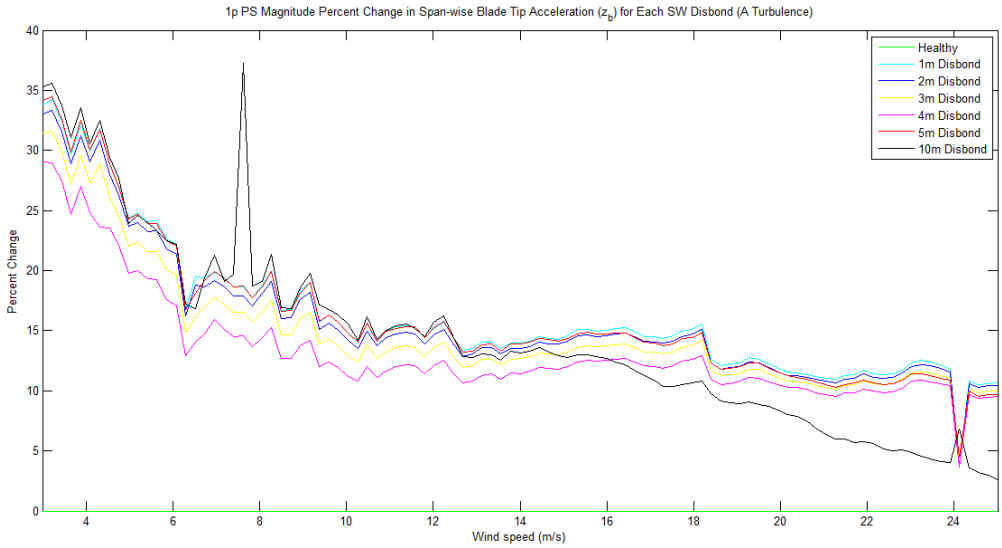

Figure 29. 1p magnitude percent change of span-wise blade tip acceleration for shear web disbond in A turbulence.

The flap-wise blade tip acceleration RMS response differences are shown in Figures 30 and 31. For all wind loading cases, there was a clear decrease in the RMS response at the turbine's rated speed (11/4 m/s) for shear web disbond lengths of 2 meters or greater. The trend of a decreased flap-wise blade tip acceleration RMS response was apparent at rated speed for all of the FAST simulations conducted in this study. In addition, the RMS response decreased as the shear web disbond length was increased. Therefore, this measurement can serve as a feature to indicate shear web disbond severity.

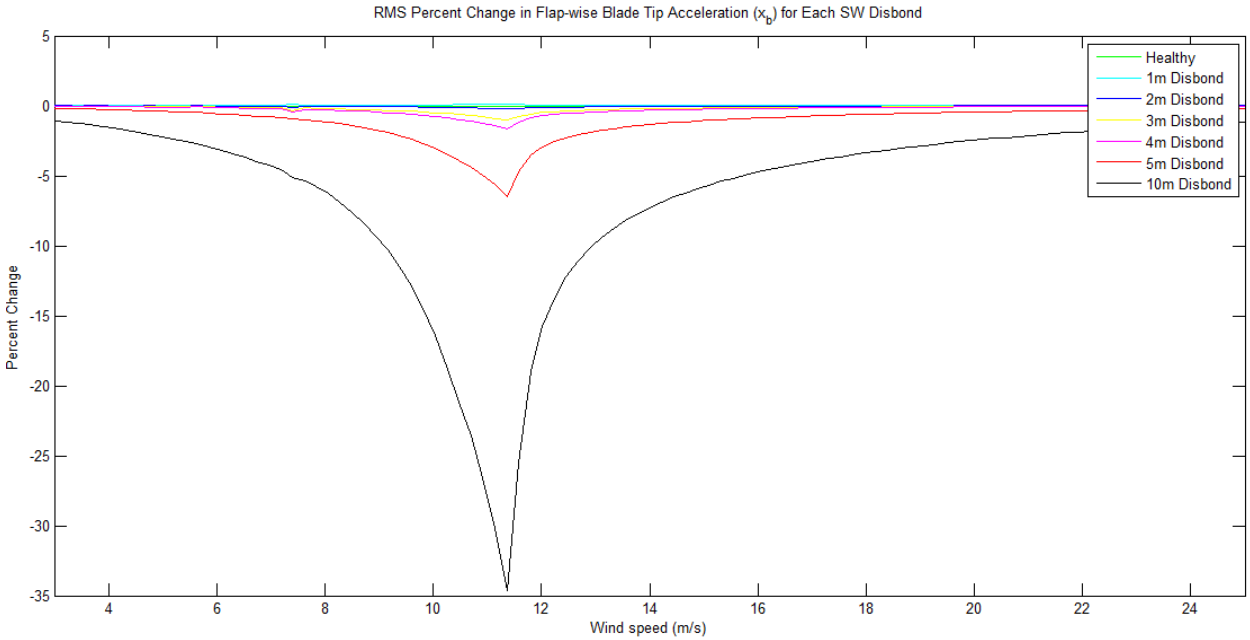

Figure 30. RMS percent change of flap-wise blade tip acceleration for shear web disbond in varying wind speeds.

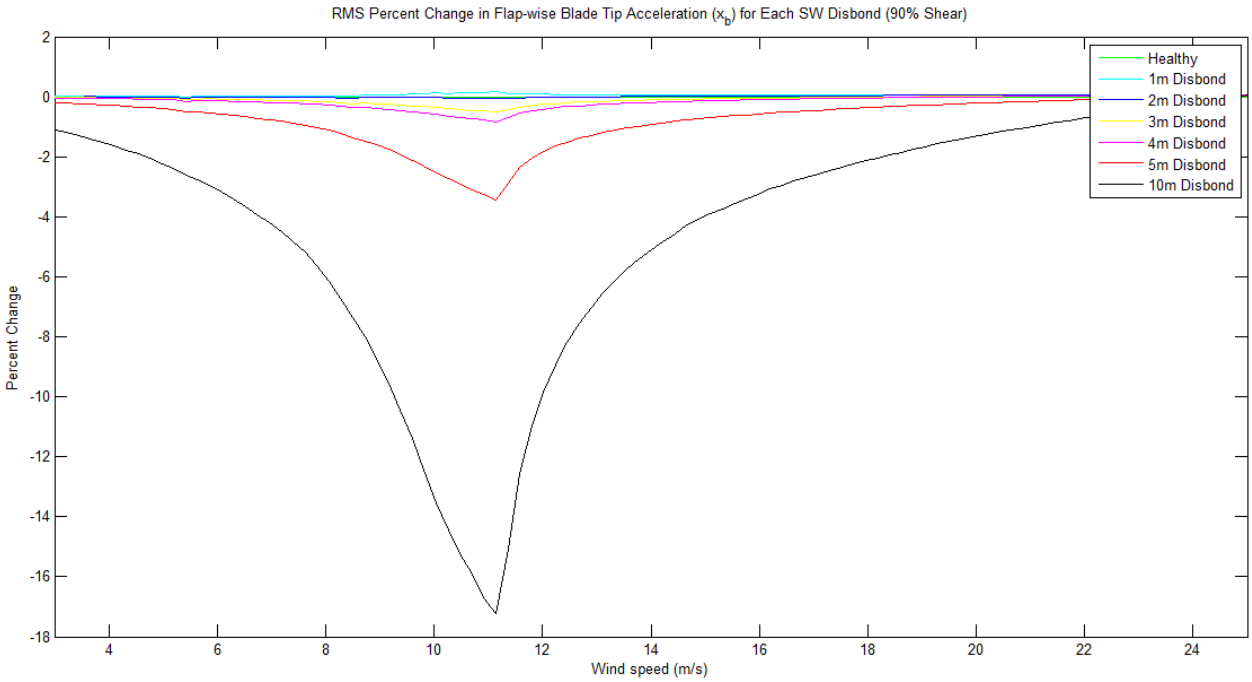

Figure 31. RMS percent change of flap-wise blade tip acceleration for shear web disbond in 90% horizontal shear.

5.4.1.4. Blade Root Pitching Moments

Figures 32 and 33 show the blade root pitching moment 1p response differences for the laminar and B turbulence wind loading cases. For all of the wind cases up to a wind speed of 16 m/s, the 1p response increased for a 4 meter, 5 meter, and 10 meter shear web disbond. This measurement can be used as another indicator that a severe shear web disbond is present in one of the blades. The blade root pitching moment can be measured with strain gages located at the root of each blade.

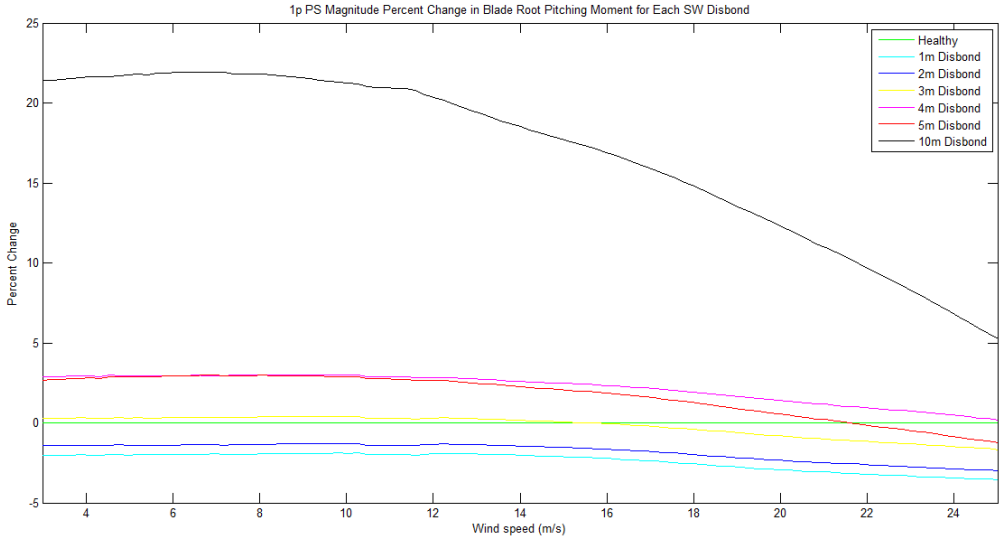

Figure 32. 1p magnitude change of blade root pitching moment for shear web disbond in varying wind speeds.

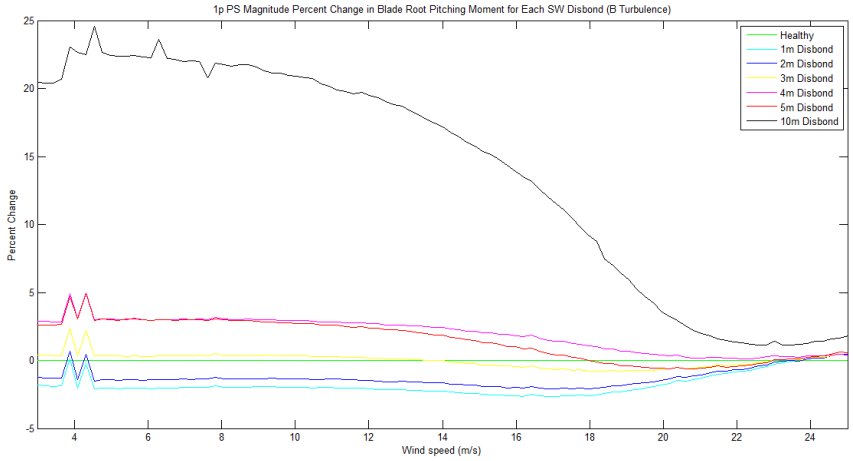

Figure 33. 1p magnitude change of blade root pitching moment for shear web disbond in B turbulence.

5.4.1.5. Blade Root Acceleration Response

The edge-wise and flap-wise blade root acceleration responses did not present any clear features when the RMS and 1p power spectrum responses were analyzed. The flap-wise blade root acceleration 1p response magnitude increased for all shear web disbonds after the rated speed of the turbine, but this trend did not continue for the horizontal shear and turbulent wind loading cases. Figures 34 and 35 shows the blade root acceleration 1p response differences for varying wind speeds and 60% horizontal shear, respectively. Other than the 10 meter shear web disbond, the span-wise blade root acceleration 1p response increased for all damage types for all wind loading cases and most of the wind speed distribution. This measurement could be used as another indicator that a shear web disbond is present at max chord. However, this feature will likely be less sensitive to a shear web disbond located further along the span of the blade because the blade root has such a high stiffness.

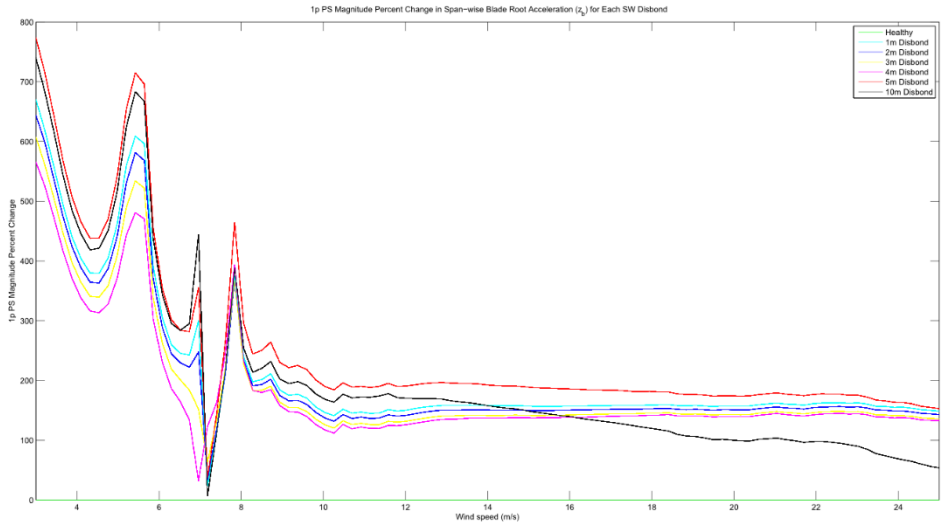

Figure 34. 1p magnitude change of span-wise blade root acceleration for shear web disbond in varying wind speeds.

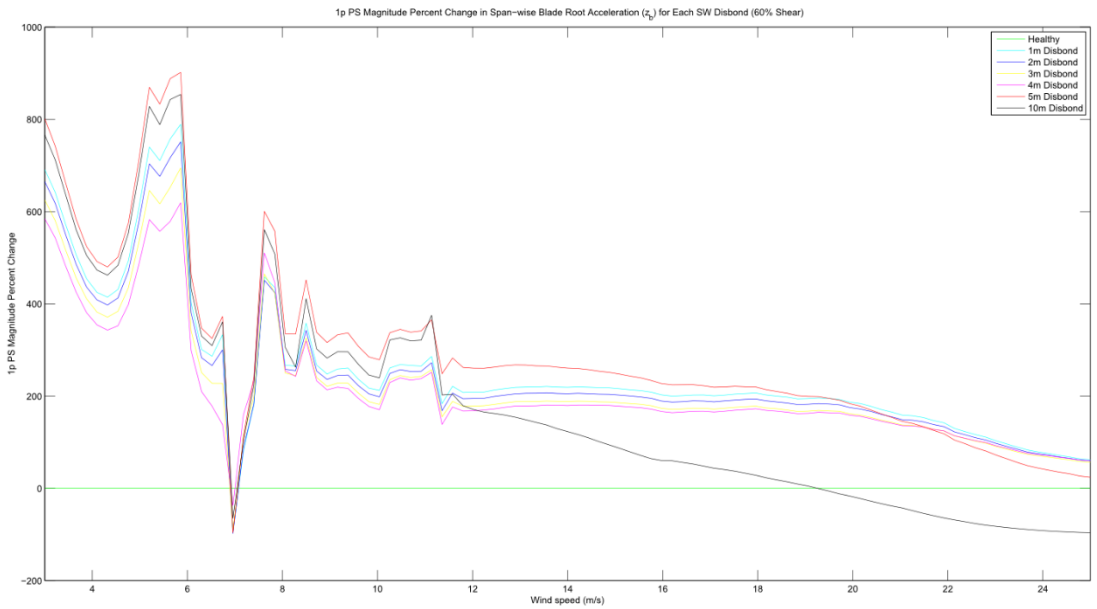

Figure 35. 1p magnitude change of span-wise blade root acceleration for shear web disbond in 60% horizontal shear.

5.5 Summary of Shear Web Disbond Detection Strategy Refinements

The results of the sensitivity analysis and key measurements have been used to refine the shear web disbond detection strategy flowchart originally shown in Figure 36. This strategy employs both blade and non-blade sensor measurements. Specifically, non-blade sensor measurements are used as the first indicator that a shear web disbond may be present and the blade sensors are used to confirm that the damage is present and its level of severity. Using a single sensor measurement to first identify potential damage will drastically reduce the necessary amount of processing and data flow *in situ*. The same action strategy will be used, as shown:

(1) Detect if a shear web disbond exists in one of the blades
(2) Determine the severity of the shear web disbond
(3) Notify turbine operator of the disbond and severity so that a repair can be scheduled or coordinated with other maintenance

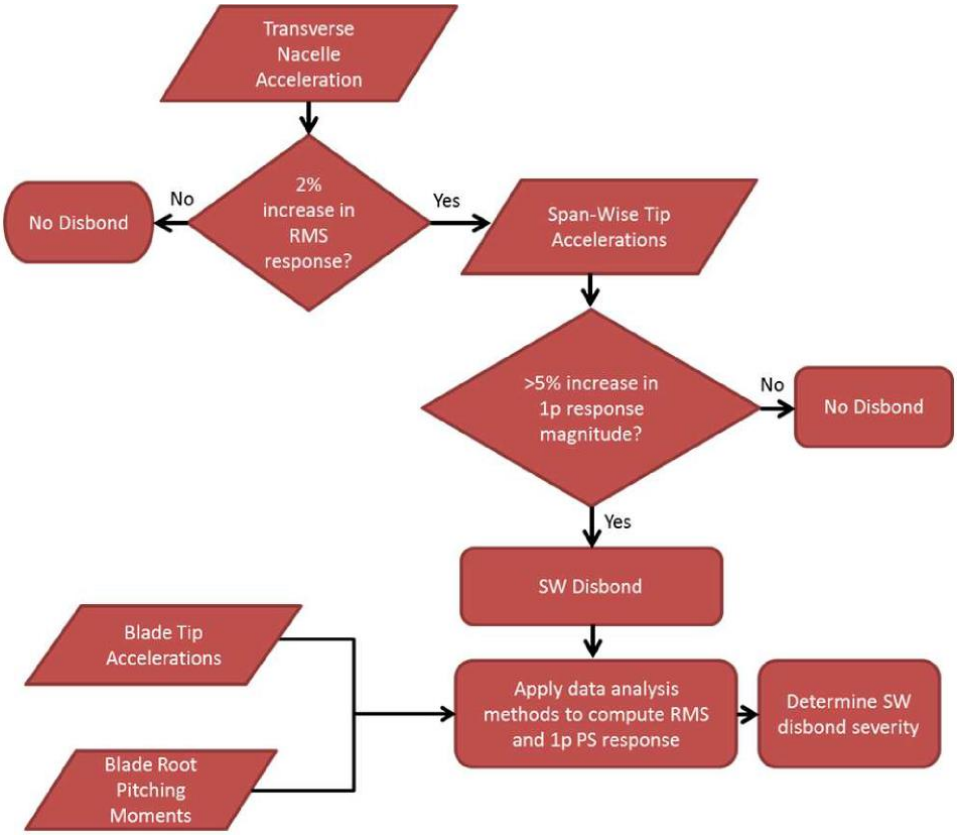

Figure 36. Refined shear web disbond detection flow chart.

The results of the sensitivity analysis and key measurements have been used to refine the shear web disbond detection strategy. This strategy employs both blade and non-blade sensor measurements. Specifically, non-blade sensor measurements are used as the indicator for a shear web disbond and the blade sensors (strain gages at the blade root) are used to detect the problematic blade and assess the level of severity. Each shear web disbond has been assigned thresholds corresponding to the severity of the damage, as shown below in Table 9.

Table 9. Shear web disbond damage state and corresponding feature used for classification

State 1 (Healthy, no disbond)	**1% increase in measured RMS transverse nacelle acceleration versus expected healthy RMS transverse nacelle acceleration**
State 2 (1, 2 meter disbond)	**1% increase in measured RMS transverse nacelle acceleration, less than 0.5% increase in 1p blade root pitching moment**
State 3 (3, 4, 5 meter disbond)	**Greater than 0.5% and less than 5% increase in 1p blade root pitching moment**
State 4 (10 meter disbond or longer)	**Greater than 5% increase in 1p blade root pitching moment**

Probability of detection values were calculated for detecting the presence of a shear web disbond in addition to detecting three different damage states which vary by severity. See Table 9 above for the damage state classifications of shear web disbond. State 2 refers to a 1-2 meter disbond, state 3 is a 3-5 meter disbond, and state 4 is a disbond of 10 meters or more. The POD values

were calculated as described in Section 4.4. If the measurement at a given wind speed, profile, and damage state met the criteria described in the tables above, then it was deemed a success. Otherwise, it was deemed a failure. For example, the blade root pitching moment is extracted from the simulation for the 3.88 m/s laminar wind profile and for a turbine with a blade which has a 4-meter shear web disbond. If there is an increase in the blade root pitching moment 1p and that increase is greater than 0.5% the healthy response and less than 5% greater than the healthy response, then the detection is a success and given a "1" value at that data point. If it does not meet the criteria, it is given a "0" value. The number of successes are then added up and that total is divided by the total number of simulations in that wind profile (101 simulations). The resultant percentage is the probability of detection for that damage state and wind profile. Table 10 shows the POD values for detecting the presence of a disbond and then categorizing the damage into each damage case, respectively. The PODs were calculated over the entire wind speed range in addition to an enhanced wind speed range which optimizes the resulting POD value for accurate damage detection for all wind loading cases. The optimized wind speed range and corresponding POD values are highlighted in green in the table. In addition, each POD value was also weighted by the Weibull distribution to incorporate the frequency of each wind speed used within the analyzed range. The POD results show that the developed algorithms are 100% successful for all of the laminar, 30% horizontal shear, and 60% horizontal shear FAST simulations. The POD values are also ~75% or greater for all but the 90% horizontal shear simulations. There is a large decrease in that probability of detection because the aerodynamic loading greatly influences the transverse nacelle acceleration response and this feature becomes the dominating feature at that measurement location rather than a shear web disbond in one of the three blades. In the real world, however, a 90% horizontal shear wind profile does not occur nearly as often as the laminar and other shear wind profiles.

Table 10. Probabilities of detection for shear web disbond

		PRESENCE OF DAMAGE		STATE 2 (1-2 m DISBOND)		STATE 3 (3-5 m DISBOND)		STATE 4 (>= 10 m DISBOND)	
		3 - 25 m/s	8.5 - 17.08 m/s	3 - 25 m/s	8.5 - 17.08 m/s	3 - 25 m/s	8.5 - 17.08 m/s	3 - 25 m/s	8.5 - 17.08 m/s
LAMINAR	Raw	84.16%	100.00%	84.16%	100.00%	83.33%	100.00%	84.16%	100.00%
	Weibull Weighted	77.24%	100.00%	77.24%	100.00%	77.16%	100.00%	77.24%	100.00%
30% SHEAR	Raw	74.26%	100.00%	72.79%	100.00%	69.11%	100.00%	72.79%	100.00%
	Weibull Weighted	78.07%	100.00%	77.95%	100.00%	77.55%	100.00%	77.95%	100.00%
60% SHEAR	Raw	44.55%	100.00%	35.73%	100.00%	36.61%	100.00%	36.17%	100.00%
	Weibull Weighted	60.18%	100.00%	58.30%	100.00%	58.61%	100.00%	58.46%	100.00%
90% SHEAR	Raw	15.84%	32.50%	10.82%	32.50%	11.29%	32.50%	10.98%	32.50%
	Weibull Weighted	25.19%	39.18%	23.21%	39.18%	23.58%	39.18%	23.34%	39.18%
A TURBULENCE	Raw	37.62%	75.00%	34.27%	75.00%	29.80%	75.00%	27.94%	75.00%
	Weibull Weighted	50.49%	74.99%	50.03%	74.99%	48.31%	74.99%	47.91%	74.99%
B TURBULENCE	Raw	45.54%	85.00%	42.39%	85.00%	36.07%	85.00%	33.82%	85.00%
	Weibull Weighted	62.86%	84.98%	61.73%	84.98%	59.38%	84.98%	59.65%	84.98%
KHTEST TURBULENCE	Raw	45.54%	80.00%	33.82%	80.00%	34.72%	80.00%	28.41%	76.00%
	Weibull Weighted	68.43%	88.06%	64.93%	88.06%	65.41%	88.06%	60.51%	85.76%

6. OPERATIONS AND MAINTENANCE COST MODEL DEVELOPMENT

This section describes the updates to the operations and maintenance cost model that was presented in Reference 17. The cost model is a state-based model that is based upon 4 states of health that decline from new blade or small damage (state 1) to failed or requiring blade replacement (state 4). There are two cases evaluated here in the model: with a SHPM system and without a SHPM system. Both cases assume the same wind conditions with the only difference being the different probabilities of detection (i.e. knowledge of state of health) for each case. The objective is to make a connection between the performance of the SHPM system with the overall economics (see Figure 7 on Page 18 for a flowchart describing this approach). Although more work remains, this section describes an update to our approach to demonstrate and better understand the impacts of the SHPM system performance (namely POD values for the system) to O&M costs and how these costs vary with POD value and wind speed.

In this state-based approach, the O&M costs are added up for the year for all repairs to restore the states that require repair (i.e. state 2 through state 4) back to state 1. The annual energy production is also calculated using the average wind speed that is modeled as a Weibull distribution with downtime included for those states requiring repair. The yearly operations and maintenance cost is divided by the annual energy production to determine the levelized cost of energy for operations and maintenance for each scenario. Finally, the cost benefit is determined by comparing the situations of with and without an SHPM system.

6.1. Introduction

The cost model has been revised in the following ways (since Reference [17]) to incorporate the wind turbine numerical simulation of damage results:

1. The probabilities of detection for the SHPM system have been revised to accept inputs from the variable inflow conditions or sensitivity analysis presented above in the aero-elastic simulations.
2. The model has been revised to consider a stochastic instead of a deterministic detection strategy.
3. The model has been created using @Risk.

6.1.1. *Model Assumptions*

The revised model accounts for the cost-benefit of increased energy production, which is an important element envisioned for these SHPM systems. The present results are focused on analysis of trends in O&M costs versus absolute O&M cost estimates. A limitation of the current model is that it does not consider unscheduled maintenance which may account for a much greater portion of the O&M costs as the literature describes that unscheduled maintenance can cost as much as five times that of scheduled maintenance. In addition, the model does not consider the benefits that may come with increased safety and possible job efficiencies associated with knowing where the defect is located on the blade before repair. Finally, there may be cost synergies between parts that have not been calculated. For instance, a gearbox may

encounter less wear if the blades are kept in balance, but additional research needs to be conducted to determine if there are any benefits due to these component interdependencies.

As such, these results should be viewed simply as a trends or sensitivity analysis -- although, they are intended to also illustrate our approach for combining SHPM system performance information into an economics analysis. Use of this model to produce absolute estimates for O&M costs in a comprehensive sense would require further refinement and inclusion of other costs such as unscheduled maintenance and actual repair costs, vessels costs, etc.

6.1.2. *Probability of Detection (POD) Revisions*

The probabilities of detection have been revised for the SHPM system to evaluate the effects of POD from the variable inflow wind turbine analysis presented above. In the original model, the probabilities of detection were assumed and were ranged from low to high values to determine the effect of varying detection probabilities. The revised probabilities have been incorporated into the current model and change with different wind speeds and wind conditions as seen in Table 11. This has caused a revision in the model to accommodate a POD that changes based upon wind speed. The PODs were arranged into six categories according to the results of the blade defect detection analysis. The PODs are shown in Table 12 showing the higher POD values with a SHPM system and lower POD values without a SHPM system. Similar to the original model, the PODs for the shear web disbond, mass imbalance, and pitch error have been aggregated and weighted according to likelihood of defect occurrence and likelihood of wind condition as noted in wind turbine blade literature. The updated cost model is still a state-based model using a Monte Carlo Markov chain although this current change adds to the randomness due to the PODs being dependent upon the wind speed which is still being modeled as a Weibull distribution where $k = 2$, $c = 11.4$, and $\beta = 1$.

Table 11. Probabilities of detection for SHPM system.

	Wind Type		
Wind Speed	Laminar	A Turb	B Turb
3	24%	12%	18%
6.74	82%	76%	94%
10.48	100%	59%	77%
14.22	100%	71%	82%
17.96	100%	0%	0%
21.7	100%	6%	0%

Table 12. Weighted Probabilities of detection for SHPM and non-SHPM systems.

	With SHPM	Without SHPM		
Wind Speed	All states	State 2	State 3	State 4
3	21%	5%	10%	16%
6.74	83%	21%	41%	62%
10.48	89%	22%	44%	67%
14.22	92%	23%	46%	69%
17.96	66%	17%	33%	50%
21.7	67%	17%	34%	50%

6.1.3. *Stochastic Detection Strategy*

The model has also been revised to use a stochastic detection strategy. This detection strategy has been modeled as a binomial distribution with the mean set to the POD. In order to incorporate this strategy, the Markov Chain has been changed from an ergodic chain to a terminating chain. The ergodic chain was modeled to only allow the blade to transition from a degraded step to a "new/repaired" state when repaired or from a less degraded state to a more degraded step to imitate the blade deteriorating. The detection process was actually part of the Markov chain (the probability that a blade in states 2, 3, or 4 will return to 1) instead of a separate step. In the revised model, the Markov Chain is terminating which means if the model runs long enough, the model will always continue to degrade until it is in a failed state and once in this failed state it will remain in that state permanently. The main difference between the two model types is that the original model can be run continuously since it can return to state 1 from other states and go through the cycle again, whereas the current model will remain in the absorbing state 4 once a sufficient amount of iterations has been reached. In the current model, the blade is only repaired if it is detected by the POD that is modeled as a binomial distribution. This change has two benefits: it is more realistic as a separate process that checks for defects and it can incorporate multiple PODs since a model can get unstable if multiple Markov Chains are used. Although the PODs have changed, the top level probabilities have remained unchanged. The assumption that the blade is repaired once the defect is detected is still valid for the current model.

6.1.4. *@Risk Model*

The model is now in the software tool @Risk. @Risk is Excel based software that is used for many commercial financial applications and cost benefit analysis. @Risk automatically incorporates multiple iterations which facilitates the Monte Carlo process and allows for inputs to easily be entered as a probability distribution. @Risk was chosen since it was designed for applications such as this cost model and allows for easy input and scenario variation. The model was shortened to one year to improve model run times in @Risk. A simulation was run changing the initial state to determine how the shortened model may impact the results since a longer model usually has years that do not start out at state 1. The results through ANOVA showed that there were no statistically significant differences between the different initial states.

6.2. Economic Sensitivity Analysis

An economic sensitivity analysis involves changing input parameters to see what influence the change has on the cost (or the cost savings in this case). The previous economic sensitivity analysis altered the operations & maintenance cost, probability of detection/repair rate, and performance coefficient to see their effects on the cost savings. The previous results showed that there were more cost savings as the disparity between the large crack repair and small crack repair increased, as the repair rate decreased, and to a lesser effect when the performance coefficient decreased. This year, the mean wind speed and the POD difference were changed between the baseline and SHPM system in addition to the changes considered last year. Altering the wind speed is useful since the current PODs change with wind speed. The other parameter that was altered was the percent difference between the baseline and the SHPM system. Since each baseline system will have a different level of detection based upon the instrumentation installed and how the collected data is used, this parameter was changed to determine how much of a change can be seen as the difference increases.

6.2.1. *Changing Mean Wind Speed*

The mean wind speed for the Weibull distribution was altered from 3 m/s to 25 m/s in increments of 2 m/s. The resulting annual energy production and levelized operations and maintenance costs were evaluated.

6.2.2. *Changing Baseline POD*

The baseline PODs were determined as a percentage of the PODs for the SHPM system for each state. The percentages were ranged from 0% to 100% for each state. They were varied one at a time with the remaining states containing the baseline values.

6.3. Simulation Results

The trends were the same as before for the parameters changed during the initial phase of the cost model. The results for the changing mean wind speed can be seen in Figures 37 and 38. The difference in annual energy production due to the SHPM system is a result of assumed decreased downtime based on the damage mechanisms (rotor imbalance, shear web disbond) and developed detection strategies shown in Sections 4 and 5. Without SHPM, the severity of damage due to rotor imbalance and/or shear web disbond is assumed to progress over time within the cost model until the blade is in a failed state.

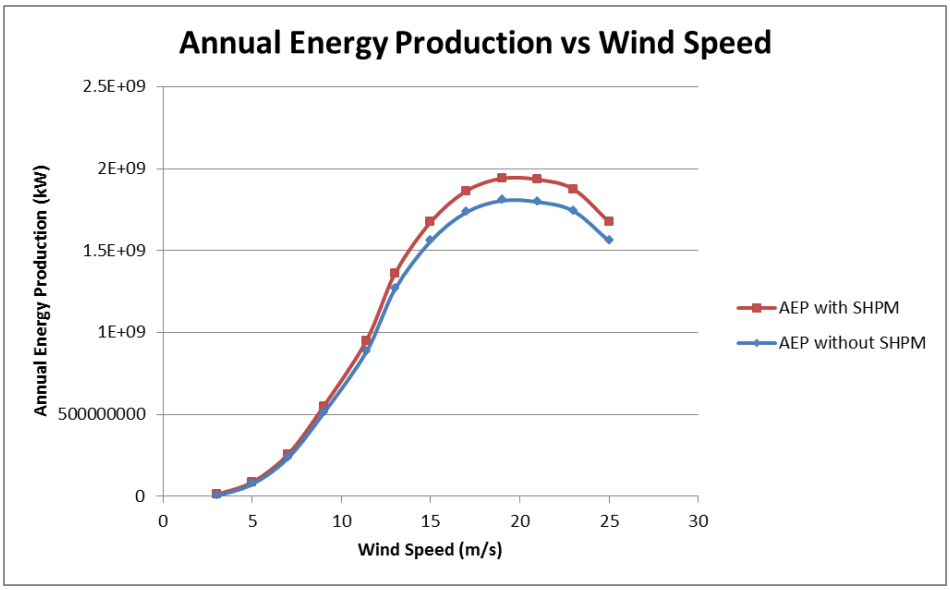

Figure 37. Annual Energy Production versus Wind Speed

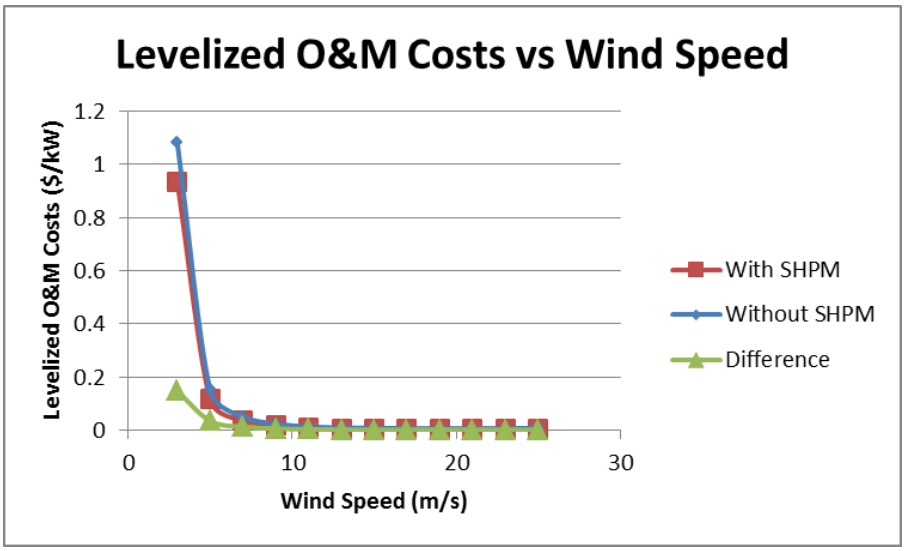

Figure 38. Levelized O&M Costs versus Wind Speed

Figure 38 shows how the levelized O&M Costs in the current model are affected by wind speeds. There is not much difference in the levelized costs for these assumptions once the wind speed surpasses 7 m/s. The SHPM blade system has either equal or slightly lower costs for most of the wind speeds.

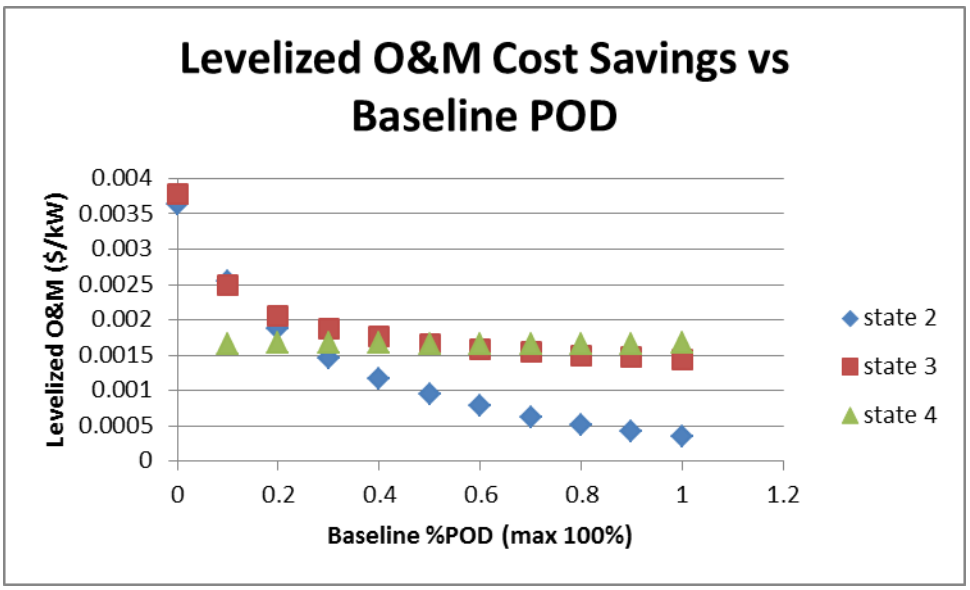

Figure 39. Levelized O&M Cost Savings versus Change in Baseline POD

Figure 39 shows the results of varying the Baseline POD based upon the SHPM POD. The POD for state 2 impacts the levelized O&M more than the POD for states 3 and 4. Although the absolute values for this current model are very small in comparison to actual O&M costs of today, the trends show the relative benefit of higher probability of detection (POD) for reducing O&M costs.

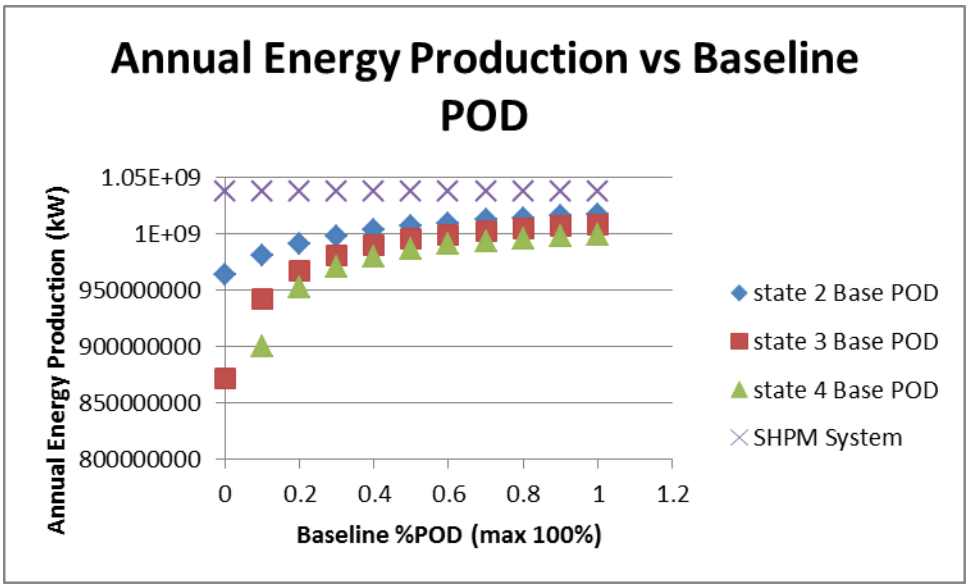

Figure 40. Annual Energy Production vs Change in Baseline POD.

Figure 40 shows the annual energy production when the baseline POD is changed. The PODs that had the highest levelized O&M have the lowest annual energy production. This is caused by the baseline POD at 0% where not being able to the detect damage early results in lower annual energy production. As the PODs improve, the energy production increases.

The cost savings seen in this economic sensitivity analysis are small in an absolute sense. Although refinement is needed, this model has been useful to identify some of the key parameters from the SHPM system that affect cost. These limitations can be addressed in future work by including refined/actual O&M costs data such as comparing planned and unplanned maintenance costs for an offshore wind farm.

7. CONCLUSIONS

A multiscale methodology[12] has been expanded for the investigation and development of structural health and prognostics management (SHPM) methods for offshore wind turbines. The method utilizes the propagation of damage from a high fidelity component level model up to a reduced order model of a full turbine so that the changes in the turbine's operational responses can be examined. Furthermore, these full turbine simulations can be used to replicate fault mechanisms such as pitch error and estimate the loads on the turbine blades which can then be propagated back to the high fidelity model to allow for further local analyses to be conducted. By investigating the effects of damage on multiple scales, the developed methodology takes advantage of available software to investigate the underlying physical changes that occur as a result of damage/faults on both a local and global level which leads to the identification of operational responses that are most sensitive to these physical changes. In turn, fault detection strategies have been developed to help optimize operations and maintenance schemes.

This report has described the application of the developed methodology to investigate rotor imbalance and shear web disbond and their sensitivities to inflow conditions on an offshore 5-MW wind turbine. The 61.5 meter blade model was developed in SNL's NuMAD software and exported to ANSYS where the shear web disbond was simulated by separating the nodes of the shear web from the blade at the location of the disbond. The reduced order blade models with varying levels of damage were included into a model of an offshore turbine on a fixed monopile in 20 meters of water. The response of these offshore turbine models with varying levels of damage/imbalance was then simulated in FAST over a wide range of wind speed, horizontal shear, and turbulence. From these simulations the detection strategies developed in the pilot study could be updated and robust probabilities of detection were derived as an algorithm success metric. For all three fault mechanisms, the probability of detection was 96% or higher for the optimized wind speed ranges including the laminar, 30% horizontal shear, and 60% horizontal shear conditions.

To examine how the structural health of each turbine could be used to optimize the operation and maintenance practices of an offshore wind plant, a state-based cost model was developed to investigate the operations and maintenance costs due to the fault/damage. The cost model compared the cost advantages of employing a SHPM system through the probability of detection values derived in the FAST sensitivity analysis. Although the model contains several assumptions, the results showed a foreseeable benefit to owning such a SHPM system; the SHPM system produced an increase in the annual energy production as well as a decrease in the levelized operations and maintenance costs. The combination of the repair cost information and the structural health of each turbine could be utilized in the optimization of damage mitigating

control strategies and maintenance schedules to reduce the operations and maintenance costs associated with running an offshore wind energy plant. The hope is that combining the SHPM system performance information with an economics analysis of the O&M process will be useful not only to motivate the greater usage of SHPM systems in wind turbine systems, but to also aid in the holistic design of such monitoring systems and the associated best maintenance practices.

8. FUTURE WORK

In future work, the algorithms developed for the 5-MW offshore turbine model could be experimentally validated on a small horizontal-axis wind turbine or utility-scale machine. The pitch error, mass imbalance, and blade damage can be introduced in order to assess the turbine's power performance, loads at the blades and nacelle, and detection of those fault mechanisms. In addition, rotor imbalance and blade damage can be detected in the presence of disturbances such as yaw error and pitch error in addition to other inflow variability from laminar to horizontal shear inflow conditions including a sweep across all operating wind speeds.

9. REFERENCES

[1] A.C. Levitt, W. Kempton, A.P. Smith, W. Musial and J. Firestone, "Pricing offshore wind power." *Energy Policy* (In Press) 2011.

[2] W. Musial and B. Ram, *Large-Scale Offshore Wind Energy for the United State: Assessment of Opportunities and Barriers*, NREL Report No. TP-500-49229, Golden, CO, September 2010.

[3] U.S. Department of Energy, *A National Offshore Wind Strategy: Creating an Offshore Wind Energy Industry in the United States,* Washington: Wind & Hydropower Technologies Program Report No. 5040, February 2011.

[4] R. Wiser and M. Bolinger, *2010 Wind Technologies Market Report*, Lawrence Berkeley National Laboratory: Lawrence Berkeley National Laboratory. LBNL Paper LBNL 4820E, June 2011.

[5] B. Snyder and M.J. Kaiser, "Ecological and economic cost-benefit analysis of offshore wind energy." *Renewable Energy* 34(6), pp. 1567-1578, 2009.

[6] G. van Bussel, A.R. Henderson, C.A. Morgan, B. Smith, R. Barthelmie, K. Argyriadis, A. Arena, G. Niklasson, and E. Peltola, "State of the Art and Technology Trends for Offshore Wind Energy: Operation and Maintenance Issues," *Offshore Wind Energy EWEA Special Topic Conference*, Brussels, Belgium, December 2001.

[7] L.W.M.M. Rademakers, H. Braam, M.B. Zaaiger, and G.J.W. van Bussel, "Assessment and optimisation of operation and maintenance of offshore wind turbines," in *Proceedings of the European Wind Energy Conference*, Madrid, Span, June 2003.

[8] Y. Amirat, M.E.H Benbouzid, B. Bensaker, and R. Wamkeue, "Condition monitoring and fault diagnosis in wind energy conversion systems: a review." In *Proceedings 2007 IEEE International Electric Machines and Drives Conference*, Vol 2., pp. 1434-1439, 2007.

[9] J. Nilsson and L. Bertling, "Maintenance management of wind power systems using condition monitoring systems – Life cycle cost analaysis for two case studies," *IEEE Transactions on Energy Conversion* 22(1), pp. 223-229, 2007.

[10] C.C. Ciang, J.R. Lee, and H.J. Bang, "Structural health monitoring for a wind turbine system: a review of damage detection methods." *Measurement Science and Technology* 19(12), pp. 1-20, 2008.

[11] F. Besnard, K. Fischer, and L. Bertling, "Reliability-centred asset maintenance – A step towards enhanced reliability availability and profitability of wind power plants" in *2010 IEEE PES Innovative Smart Grid Technologies Conference Europe (ISGT Europe)*, 2010.

[12] Z. Hameed, S.H. Ahn, and Y.M. Cho, "Practical aspects of a condition monitoring system for a wind turbine with emphasis on its design, system architecture, testing and installation," *Renewable Energy*, 35(5), pp. 879-894, May 2010.

[13] NWTC Design Codes (FAST by Jason Jonkman, Ph.D.). http://wind.nrel.gov/designcodes/simulators/fast/. Last modified 05-November-2010; accessed 05-November-2010.

[14] R.R. Ryan, ADAMS – Multibody System Analysis Software, Multibody Systems Handbook. Berlin: Springer-Verlag, 1990.

[15] J. Jonkman, S. Butterfield, W. Musial, and G. Scott, "Definition of a 5-MW Reference Wind Turbine for Offshore System Development," NREL/TP-500-38060, Golden, CO: National Renewable Energy Laboratory, February 2009.

[16] D.T. Griffith, N. Yoder, B. Resor, J. White, and J. Paquette, "Structural Health and Prognostics Management for Offshore Wind Turbines: An Initial Roadmap," Sandia

National Laboratories Technical Report, SAND2012-10109, Sandia National Laboratories; Albuquerque, NM, Printed December 2012.
[17] N. Myrent, J. Kusnick, N. Barrett, D. Adams, and D.T. Griffith, "Structural Health and Prognostics Management for Offshore Wind Turbines: Case Studies of Rotor Fault and Blade Damage with Initial O&M Cost Modeling," Sandia National Laboratories Technical Report, SAND2013-2735, Sandia National Laboratories; Albuquerque, NM, Printed April 2013.
[18] J. Jonkman and L. Buhl, "FAST User's Guide," NREL/EL-500-38230, Golden, CO: National Renewable Energy Laboratory, August 2005.
[19] J. Giebhardt and WP7 Partners, "Condition Monitoring for Wind Turbines 'State of the Art' Report," Kassel, Germany: European Commission, 2007.
[20] IEC 61400-1, "Wind turbine generator systems-Part 1: Safety requirements," 2nd edition, Geneva, Switzerland: International Electrotechnical Commission, 1999.
[21] B.J. Jonkman and L. Kilcher, "TurbSim User's Guide: Version 1.06.00," NREL/TP-xxx-xxxx (Draft Version), Golden, CO: National Renewable Energy Laboratory, September 2012.
[22] C. A. Walford, Wind turbine reliability: understanding and minimizing wind turbine operation and maintenance costs: United States. Department of Energy, 2006.

ACKNOWLEDGEMENT

This work was funded by the US Department of Energy (DOE), Office of Energy Efficiency and Renewable Energy (EERE), Wind and Water Power Technology Office.

Distribution:

5 Cecelia Sterling
Office of Wind and Hydropower Technologies
EE-2B Forrestal Building, U.S. DOE
1000 Independence Ave. SW
Washington, DC 20585

5 Library NWTC
NREL/NWTC
1617 Cole Boulevard
Golden, CO 80401

Internal Distribution

10	MS1124	D.T. Griffith	Org. 6122
10	MS1124	Wind Library	Org. 6121
1	MS0899	Technical Library	9536 (electronic copy)


Sandia National Laboratories